Metamorphic Processes

3

Sagvandite outcrop at the type locality Sagelvvatnet, Norway. Radial bundles of large enstatite crystals with interstitial magnesite. The rock formed by carbonation of dunite. It is an example of natural CO_2 sequestration

K. Bucher, *Petrogenesis of Metamorphic Rocks*, Springer Textbooks in Earth Sciences, Geography and Environment,
https://doi.org/10.1007/978-3-031-12595-9_3

Metamorphism reworks existing rocks. The starting material, protolith, is being transformed and altered to something new, the new metamorphic rock. The reworking is caused by changing external conditions such as temperature, lithostatic pressure, stress, chemical forces and other parameters. Metamorphism is related to chemical and mechanical processes. The chemical processes change predominantly the mineral assemblage making up the rock and also may change the chemical composition of the rock. The mechanical processes change predominantly the fabric and structure of a rock. Chemical and mechanical processes are strongly interrelated. Stress and the resulting strain modify the transport properties of the rocks and influence the kinetics of metamorphic reactions.

Typical results of metamorphic processes include:

- Minerals and mineral assemblages originally not present in a rock may form, the new mineral assemblages grow at the expense of old ones. Consequently older minerals may disappear. For example: A metapelitic gneiss may originally contain Sil + Grt + Bt. A metamorphic event transforms this rock into one that contains Crd + Grt + Bt in addition to Qtz and Fsp that also have been previously present in the rock; the old rock contained Sil, the new one Crd (Figs. 3.1, 2.14).
- Metamorphic minerals may systematically change their composition (e.g. the X_{Mg} of Grt and Crd may simultaneously increase during metamorphism) (Fig. 2.14, e.g. AFM triangle rotation).
- The relative abundance of minerals in a rock may systematically change and the new rock may have a different modal composition (metamorphism may increase the amount of Crd present in the rock and decrease the volume proportion of Grt + Bt) (Fig. 2.14 e.g. AFM triangle rotation).
- The structure of rocks in crust and mantle may be modified (e.g. randomly oriented biotite flakes may be parallel aligned after the process).
- The composition of the bulk rock may be altered during metamorphism by adding or removing components to, or from the rock from a source/sink outside the volume of the rock considered (e.g. removing K_2O, MgO and FeO dissolved in a coexisting aqueous solution from a Grt + Crd + Bt rock may result in the formation of sillimanite) (Fig. 2.14; moving the rock composition specified by the blue spot into the Sil + Grt + Crd field).

Typical changes in the modal composition of rocks and in the chemical composition of minerals that constitute the rocks are caused by heterogeneous chemical reactions progressing in the rocks. The principles of metamorphism are, therefore, strongly related to the principles of chemical reactions. Mineral- and rock-forming metamorphic processes are mainly controlled by the same parameters that control chemical reactions. Metamorphic petrology studies reaction and transport processes in rocks. Metamorphic processes are caused by transient chemical, thermal and mechanical disequilibrium in confined volumes of the Earth's crust and mantle. These disequilibrium states ultimately result from large-scale geological processes and the dynamics of the Earth's planetary system as a whole. Metamorphic processes always result from disequilibrium and gradients in parameters that control

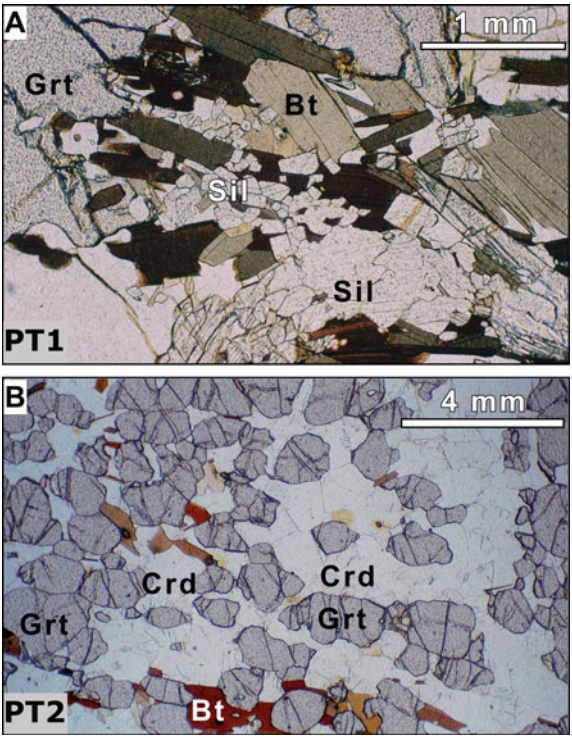

Fig. 3.1 Metapelitic gneiss from two different locations in the Thor Range (Antarctica) (Bucher-Nurminen and Ohta 1993). **a** Grt + Bt + Sil, **b** Grt + Bt + Crd. Note yellow halo of radiation damage in cordierite caused by small zircon grains (the halos are black in biotite). The two assemblages are connected by the discontinuous reaction Sil + Bt = Grt + Crd balanced with Qtz + Kfs + H_2O which are/were present in excess (see AFM diagram Fig. 2.14)

reaction and transport in rocks; they cease when the rocks reach an equilibrium state. Chemical reaction is always inherent in the term metamorphism. The term metamorphosis actually means transformation, modification, alteration, and conversion and thus is clearly a process-related expression.

Metamorphism is a very complex occurrence that involves a large number of chemical and physical processes at various scales. Metamorphic processes can be viewed as a combination of (1) chemical reactions between minerals and between minerals and gasses, liquids and fluids (mainly H_2O) and (2) transport and exchange of substances and heat between domains where such reactions take place. The presence of an aqueous fluid phase in rocks undergoing metamorphism is critical to the rates of both chemical reactions and chemical transport. Consequently, an advanced understanding of metamorphism requires a great deal of insight into the quantitative description of chemical reactions and chemical transport processes, especially reversible and irreversible chemical thermodynamics.

The term metamorphism as it is related to processes, changes and reactions clearly also includes the aspect of time. Metamorphism occurs episodically and is particularly related to mountain-building or orogenic episodes at convergent plate margins (collision zones) and during subsequent uplift and extension of continental crust, but also during sea-floor spreading and continental rifting.

3.1 Principles of Metamorphic Reactions

The following introductory account of some basic aspects of metamorphic reactions and selected elementary principles helps providing a basic appreciation of metamorphism. The treatment is not sufficient for a thorough understanding of metamorphic processes and chemical reactions in rocks. It is therefore recommended for the reader who needs to know more, to study textbooks on chemical thermodynamics (e.g. Guggenheim 1986; Lewis and Randal 1961; Moore 1972; Prigogine 1955; Denbigh 1971) or textbooks that deal particularly with the application of thermodynamics to mineralogy and petrology (Ferry 1982; Fraser 1977; Greenwood 1977; Lasaga and Kirkpatrick 1981; Powell 1978; Saxena and Ganguly 1987; Wood and Fraser 1976). Particularly recommended treatment of the topic: Chatterjee (1991), Fletcher (1993), Norstrom and Munoz (1994), Anderson and Crerar (1993), and Ganguly (2008).

First, let us consider, for example, a rock that contains the minerals albite and quartz. The Ab-Qtz rock is located at a certain depth in the crust (e.g. at point T_h = 1.25 GPa, 550 °C in Fig. 3.2). At that given pressure and temperature the two minerals (phases) are associated with unique values of molar Gibbs free energy. The Gibbs free energy, usually abbreviated with the symbol **G**, is a thermodynamic potential with the dimension Joules/mole (energy/mole) and it is a function of pressure and temperature. The free energy of minerals and their mixtures are negative quantities (because they refer to the free energy of formation from the elements or oxides rather than absolute energies, e.g. G of albite at 900 K and 0.1 MPa is −3257.489 kJ $mole^{-1}$). The considered Ab + Qtz rock can be formed by mechanically mixing, for example, 1 mol albite and 1 mol quartz. All rocks represent, thermodynamically speaking, mechanical mixtures of phases and are therefore heterogeneous thermodynamic systems.[1] The phases, in turn, can be viewed as chemically homogeneous sub-spaces of the considered system, e.g., a volume of rock. Minerals, aqueous fluids, gasses and melts are the thermodynamic phases in rocks. These phases are usually chemical mixtures of a number of phase components (most minerals are solid chemical solutions and show a wide range in composition). In our example, albite and quartz shall be pure $NaAlSi_3O_8$ and SiO_2 respectively. The total free energy of the rock is the sum of the free energies of its parts, that is in our case, $n_{Ab}G_{Ab} + n_{Qtz}G_{Qtz}$ (where n_i = number of moles of

[1] The thermodynamic description of heterogeneous systems has been developed and formulated mainly by W. Gibbs (Gibbs, 1878; Gibbs, 1906). Gibbs scientific contributions were fundamental for the development of modern quantitative petrology.

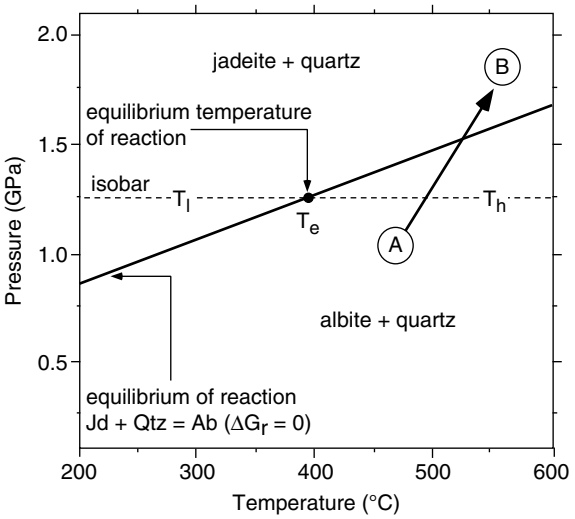

Fig. 3.2 Pressure—temperature diagram showing equilibrium conditions of the reaction jadeite + quartz = albite

substance i). The rock is characterized by a unique value of **G** and, by taking one mole of each substance; its total composition is $NaAlSi_4O_{10}$. However, the composition of such a mechanical mixture (≡ rock) can also be obtained by mixing (powders of) jadeite ($NaAlSi_2O_6$) and quartz in the appropriate proportions. It is clear also that this rock has a unique Gibbs free energy at the given pressure and temperature and that it corresponds to the sum of $G_{Jd} + 2\ G_{Qtz}$. The free energy of the Ab-Qtz rock may be designated G_{AQ} and that of the Jd-Qtz rock G_{JQ}. The Gibbs free energies of the two rocks at P and T can be calculated from Eqs. (3.1) and (3.2) provided that the free energy values of the three minerals can be calculated for that P and T:

$$G_{AQ} = G_{Ab} + G_{Qtz} \tag{3.1}$$

$$G_{JQ} = G_{Jd} + 2\ G_{Qtz} \tag{3.2}$$

The Gibbs free energy of the three minerals at P and T can be calculated from thermodynamic data and equations of state given by the laws of chemical thermodynamics. The question one may ask now is, which one of the two possible rocks, the albite + quartz rock or the jadeite + quartz rock, will be present at the conditions T_h (Fig. 3.2). According to the thermodynamic laws it is always the mixture with the lowest total free energy at the prevailing conditions that is the **stable** mixture (assemblage) while the other mixture is **metastable**. These laws can be summarized and expressed by the following statement:

The chemical components (constituents) making up the bulk composition of a rock are distributed into a group of homogeneous phases, (minerals and fluid(s)), that constitute the assemblage with the lowest Gibbs free energy for the system at

that given pressure and temperature. This assemblage is called the **equilibrium phase assemblage**.

At T_h, G_{AQ} is more negative than G_{JQ} and thus the albite + quartz rock is stable, while the jadeite + quartz assemblage is metastable or less stable than Ab + Qtz. The free energy difference of the two rocks can be calculated by subtracting Eq. (3.2) from Eq. (3.1):

$$\Delta G = G_{AQ} - G_{JQ} = G_{Ab} - G_{Jd} - G_{Qtz} \tag{3.3}$$

ΔG is the free energy difference of the two rocks with identical composition but different mineral content. The minerals of the two rocks are connected by a reaction that can be expressed by the stoichiometric equation:

$$\underset{\text{jadeite}}{1\ NaAlSi_2O_6} + \underset{\text{quartz}}{1\ SiO_2} = \underset{\text{albite}}{1\ NaAlSi_3O_8} \tag{3.4}$$

The stoichiometric coefficients in this particular reaction equation are all equal to 1. The equation suggests that albite in the Ab + Qtz rock that is stable at T_h may decompose to jadeite + quartz at some other conditions than T_h. Similarly, the reaction Eq. (3.4) describes the formation of 1 mol Na-feldspar from 1 mol jadeite + 1 mol quartz. The free energy change of the reaction ΔG_r is calculated from:

$$\Delta G_r = G_{Ab} - G_{Jd} - G_{Qtz} \tag{3.5}$$

By convention, the stoichiometric coefficients on the right hand side of a reaction equation are always taken as positive, while those on the left hand side are taken as negative. In the example given here the energy difference of the two rocks (Eq. [3.3]) is identified as the free energy change of the albite-forming reaction. ΔG_r is, like G of the individual phases, a function of P and T. Three basic cases may be distinguished:

$$\Delta G_r < 0 \tag{3.6}$$

At all pressure and temperature conditions that satisfy Eq. (3.6) the products of the reaction are stable and the reactants are metastable. At T_h, ΔG_r is negative and Ab + Qtz constitute the stable assemblage. A rock with Jd + Qtz is metastable at T_h.

At all conditions that satisfy Eq. (3.7) the reactants of the reaction are stable and the products are metastable.

$$\Delta G_r > 0 \tag{3.7}$$

At T_l, ΔG_r is positive and Jd + Qtz constitute the stable assemblage (Fig. 3.2). A rock with Ab + Qtz is metastable at T_l.

At all conditions that satisfy Eq. (3.8) the reactants and products of the reaction are simultaneously stable.

$$\Delta G_r = 0 \tag{3.8}$$

These conditions are referred to as the **equilibrium conditions of the reaction**. In Fig. 3.2, the equilibrium condition of the reaction expressed by Eq. (3.8) is represented by a straight line. Along that line all three minerals are simultaneously stable. At a pressure of 1.25 GPa, the equilibrium temperature of the reaction is 400 °C and corresponds to the point T_e along the isobar of Fig. 3.2. At this unique temperature the rock may contain all three minerals in stable equilibrium. At any temperature other than T_e the reaction is not at equilibrium and it will proceed in such a way as to produce the assemblage with the most negative free energy for the given temperature. In Fig. 3.2, the equilibrium line of the reaction divides the *P–T* space into two half spaces with two distinct stable assemblages. In this way, the *P–T* diagram represents a Gibbs free energy map of the considered system. Like a topographic map where the surface of the Earth is projected along a vertical axis, a *P–T* phase diagram represents a map where the lowest Gibbs free energy surface of the system is projected along the G-axis onto the *P–T* plane.

At equilibrium, the mineralogical composition of a rock is entirely dictated by its composition, the pressure and the temperature. If temperature and pressure change, new assemblages may have a lower Gibbs free energy, and chemical reaction will replace the old assemblage by a new, more stable assemblage. A rock always tries to reach a state of equilibrium by minimizing its Gibbs free energy content. This is accomplished by readjusting the mineralogy or the composition of minerals if necessary.

Stable assemblages cannot be distinguished from metastable ones by any petrographic technique, and metastable equilibria cannot be separated from stable equilibria. This becomes obvious if we look at a rock sample collected on a rainy day that contains the three Al–silicate minerals, kyanite, andalusite, sillimanite in addition to quartz. All three Al-silicates are metastable in the presence of quartz and water under surface conditions relative to the *hydrous* Al–silicate, kaolinite. In general, at some arbitrary metamorphic *P–T* condition only one Al–silicate + quartz can be stable, the other two possible two-phase assemblages must be metastable. Metastable persistence of metamorphic minerals and assemblages is common in metamorphic rocks. This is, of course, an extremely fortunate circumstance for metamorphic petrologists. Rocks that formed in the deep crust or mantle with characteristic high-pressure and high-temperature mineral assemblages may be collected at the Earth's surface. If metastable assemblages were not common in metamorphic rocks we would find only low-*P–T* rocks at the surface. Metastable assemblages may even survive over geological time scales (hundreds of millions of years). It is obvious from Fig. 3.2 that a rock containing Jd + Qtz is metastable under conditions at the surface of the Earth. However, rocks containing Jd + Qtz are found at surface outcrops and provide evidence that they were formed originally at very high pressures.

Some criteria and methods to detect **disequilibrium** in rocks do exist, however. One may distinguish two main kinds of disequilibrium; structural or textural disequilibrium and chemical disequilibrium. Structural disequilibrium is indicated by distinct shapes and forms of crystals and spatial distribution and arrangement of groups of minerals in heterogeneous systems. Structural disequilibrium may be found in rocks that underwent chemical reactions or successive series of reactions that all ceased before equilibrium structures developed and overall chemical equilibrium was reached. For example, chemically zoned minerals with relic, often resorbed cores, representing an earlier metamorphism overgrown and partly replaced by compositionally different rims that formed during later metamorphism. Many different kinds of compositional features of metamorphic rocks and minerals may indicate chemical disequilibrium. As an illustration we can use our Jd + Qtz example again, except that in this case the rock that contains omphacite (Omp) + quartz (sodium-rich clinopyroxene where jadeite is present as a phase component). Independent information suggests that this example rock formed at about 600 ˚C. The rock may also contain pure albite in domains, local patches or veins and its composition clearly indicates chemical disequilibrium. The minerals Omp + Ab + Qtz never coexisted in stable or metastable equilibrium because the pyroxene contains a calcic component (diopside) and the feldspar does not (the phase component anorthite is not present in Pl). However, at the inferred temperature of 600 ˚C, plagioclase in an omphacite-bearing rock should, in an equilibrium situation (stable or metastable), contain some anorthite component. The presence of albite in such a rock must be related to some metamorphic process that progressed under conditions other than the equilibration of the Omp + Qtz assemblage. It is, on the other hand, important to note that the assemblage Omp + Qtz + Ab represents an overall disequilibrium but the assemblages Omp + Qtz and Ab + Qtz may well be equilibrium assemblages that equilibrated at different times at different *P–T* conditions. The question of equilibrium is always related to the scale of equilibrium domains. Disequilibrium may exist between large rock bodies in the crust, layers of rocks of different composition at an outcrop, between local domains of a thin section or between two minerals in mutual grain contact. Any chemically zoned mineral also represents disequilibrium. At some scale there is always disequilibrium at any time.

Chemical properties of coexisting minerals in a rock are often used for resolving the question of equilibrium. As an example, a series of garnet-biotite pairs have been analyzed from a homogeneous Grt-Bt schist and the data are schematically shown in Fig. 3.3. The data pairs can be arranged into two groups. *Group a* represents matrix biotite in contact with the rim of garnet; *group b* represents analyses of biotite grains included in the cores of garnet. Overall chemical equilibrium (stable or metastable) between garnet and biotite requires that both minerals have a uniform composition in the rock. Crossing tie lines are inconsistent with overall equilibrium. However, it is evident that the Grt − Bt pairs from each group are not in conflict with the requirements of chemical equilibrium. They are likely to constitute two different **local equilibrium** systems. However, the Grt − Bt pair connected with a dashed line in Fig. 3.3 shows crossing tie-line relationships within

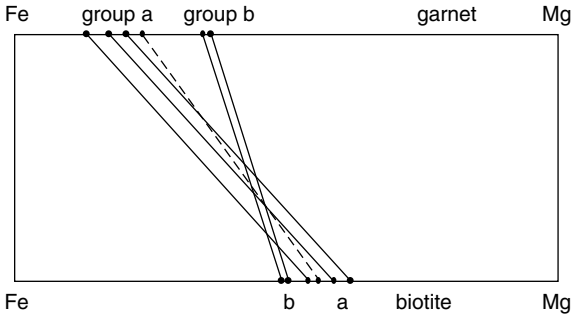

Fig. 3.3 Schematic diagram showing the Fe–Mg distribution between coexisting garnet and biotite pairs in a sample of metapelitic rock

group a pairs and clearly represents a disequilibrium pair. Note that the absence of crossing tie-line relationships does not necessarily prove that the rock was in a state of overall equilibrium. The lack of obvious disequilibrium phenomena can be taken as evidence for, but not as proof of, equilibrium.

Metastable persistence of minerals and mineral assemblages and also the obvious disequilibrium features in many rocks reflects the controlling factors and circumstances of reaction kinetics. The rate of a mineral reaction may be slower than the rate of, e.g., cooling of a volume of rock. Lacking activation energy for reaction in cooling rocks and nucleation problems of more stable minerals typically affects reaction kinetics. The kinetics of reactions in rocks is extremely sensitive to the presence or absence of H_2O. Aqueous fluids serve as both a solvent and a reaction medium for mineral reactions. For example, if kyanite-bearing rocks are brought to pressure and temperature conditions where andalusite is more stable than kyanite, kyanite may be replaced by andalusite in rocks containing a free aqueous fluid in the pore space or along grain boundaries, whilst andalusite may fail to form in fluid-absent or dry rocks.

It is commonly reasonable to assume that during **prograde** metamorphism rocks pass through successive sequences of equilibrium mineral assemblages. These sequences can be viewed as a series of stages, each of them characterized by an equilibrium assemblage and the different stages are connected by mineral reactions. This assumption is founded on convincing evidence that prograde metamorphism takes place under episodic or continuous water-present conditions. One would therefore expect to find disequilibrium and metastable assemblages particularly in rocks that were metamorphosed under fluid-absent or fluid-deficient conditions. Aqueous fluids are typically not present in cooling rocks after they have reached maximum metamorphic pressure and temperature conditions. Textural and chemical disequilibrium is also widespread in very high-grade rocks of the granulite facies that have lost their hydrous minerals and aqueous fluids during earlier stages of prograde metamorphism. Microstructures such as reaction rims, symplectites, partial replacement, corrosion and dissolution of earlier minerals are characteristic features of granulite facies rocks. They indicate that, despite relatively high

temperatures (700 to 900 °C), equilibrium domains were small and chemical communication and transport were hampered as a result of dry or H_2O-poor conditions.

To further illustrate some aspects of disequilibrium, we may consider large bodies of incompatible rock types in the crust. In many orogenic fold belts (e.g. Alps, Caledonides, Tianshan) mantle-derived ultramafic rock fragments were emplaced in the continental crust during the collision phase and stacking of nappes. Mantle fragments (harzburgite, lherzolite, serpentinite) of various dimensions can be found as lenses in granitic crust (Fig. 3.4). Forsterite (in the mantle fragment) + quartz (in the crustal rocks) is metastable relative to enstatite at any geologically accessible *P–T* conditions. The presence of Fo-bearing mantle rocks in Qtz-rich crustal rocks represents a large-scale disequilibrium feature. Chemical mass transfer across the contact of the incompatible rock types results in the formation of shells of reaction zones that encapsulate the mantle fragment. The nature of the minerals found in the reaction zones depends on the *P–T* conditions and the composition of the fluid phase at the reaction site. In our example, the reaction shells may consist of talc- and biotite-rich zones that are typically nearly monomineralic (Fig. 3.4). Biotite-, chlorite- or amphibole-rich zones that form as a result of disequilibrium on a macroscopic scale and subsequent chemical transport and reaction are also known as blackwall. The process is one of contact metasomatism, Chemical communication, transport and reaction are most efficient if aqueous fluids are present in excess and wet the grain boundaries in the incompatible rock bodies. Metasomatism proceeds until the incompatible mineralogy has been used up by the process or the rocks lose their aqueous fluid phase. In rocks with dry grain boundaries, diffusional mass transfer is extremely slow and inefficient even over geological time spans.

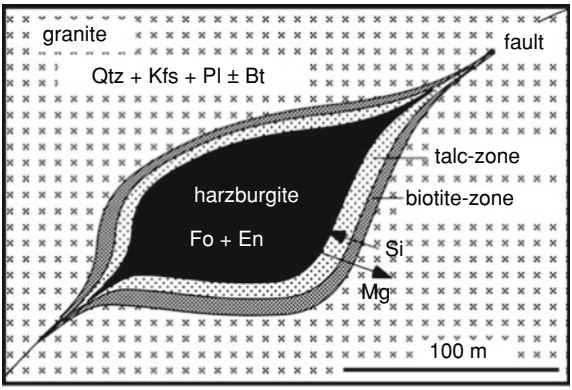

Fig. 3.4 Large-scale disequilibrium between a tectonic lens of harzburgite (ultramafic rock fragment from the upper mantle) in granitic (gneissic) crust. The harzburgite lens is enveloped by protective shells of talc and biotite. These shells were produced by chemical reaction between incompatible rocks (rocks of radically different compositions) and their formation required transfer of, e.g. Si from granite to harzburgite and Mg from harzburgite to granite

Returning again to the Jd-Qtz-Ab example. At the conditions of point A in Fig. 3.2, a rock containing Ab + Qtz is more stable than a rock composed of Jd + Qtz. Consider an Ab + Qtz rock that has reached a state of chemical and structural (textural) equilibrium at conditions of point A. The assemblage of this rock may be replaced by Jd + Qtz by reaction (3.4) if the rock is brought to the conditions at point B (increasing temperature and pressure during prograde metamorphism). It is obvious that a transfer from A to B would shift the Ab + Qtz rock into the field where Jd + Qtz represents the stable assemblage. The causes of such changes in *P* and *T* are explained in the following section.

3.2 Pressure and Temperature Changes in Crust and Mantle

3.2.1 General Aspects

Changes in pressure and temperature are the prime causes of metamorphism. This raises the question: what kind of geologic processes lead to changes in pressure and temperature in the crust or the mantle?

In a general way, such changes are caused by some force that acts on rocks (driving force: driving the process or change). Any kind of force applied to a rock will cause some flow or transfer of a property in such a way as to reduce the size of the applied force.

Temperature differences between volumes of rocks result in the transfer of heat (heat flow) from hot rock to cold rock until both rocks reach the same temperature. A simple linear equation describes this process:

$$J_Q = -L_Q \nabla T \tag{3.9}$$

Equation (3.9) states that a non-uniform temperature distribution in a system will transfer heat (Q) in the direction normal to the isotherms of the temperature field and from high temperature to low temperature in order to decrease the temperature difference. The linear equation (known as Fourier's law) describes heat flow in systems with small temperature differences (such as most geologic systems). L_Q is a material-dependent constant related to the thermal conductivity of the material κ. J_Q is the rate of heat transfer per unit area (heat flow vector) parallel to the highest gradient in the temperature field ($J_Q = \partial Q/\partial t$). ∇T represents the gradients in temperature in the three-dimensional space. If there are only linear temperature gradients in one direction, the ∇T in Eq. (3.9) reduces to $(T_{x_1} - T_{x_2})$, the temperature difference between two points. The general expression presented above shows that gradients in intensive variables in a system ultimately cause "processes" and "changes", geological or other. As metamorphism is mainly related to chemical

reactions in rocks that are largely controlled by changes in temperature, pressure and rock composition, it is useful to discuss geological aspects of heat transfer, pressure changes and chemical mass transfer in the crust and mantle in some detail.

3.2.2 Heat Flow and Geotherms

Fourier's law states that heat will be transported from a place at high temperature to an area at low temperature. In the case of the Earth, and looking at it on a large scale, there is a hot interior and a cold surface. This necessarily results in transport of heat from the center to the surface. The surface of the earth is at a nearly constant temperature (about 10 °C) and the core mantle boundary is probably also at a constant temperature as a result of the liquid state of the outer core that permits very rapid convection and heat transport. The general situation is depicted in Fig. 3.5. A consequence of the temperature difference between the two surfaces is a steady and continuous heat flow from the interior to the surface.

Heat flow is measured in Watt per square meter (W m^{-2}); however, in the literature heat flow data are often given in "HFU" (heat flow units). A HFU is defined as μcal cm^{-2} s^{-1}, that is equivalent to 4.2 μJ s^{-1} cm^{-2} or 0.042 J s^{-1} m^{-2}. Because J s^{-1} is equivalent to W (Watt), it follows that 1 HFU is equal to 0.042 W m^{-2} (or more convenient 42 mW m^{-2}).

The heat flow from the interior of the Earth is on the order of 30 mW m^{-2}. However, heat flow measurements at the surface of the Earth vary between about 30 and 120 mW m^{-2}. The total heat flow at the surface is composed of a number of contributions: (1) heat flow from the interior resulting from conductive heat transport as described by Fourier's law, (2) transport of heat by convective mass flow in the mantle (Fig. 3.6), (3) transport of heat generated by decay of radioactive elements present in minerals.

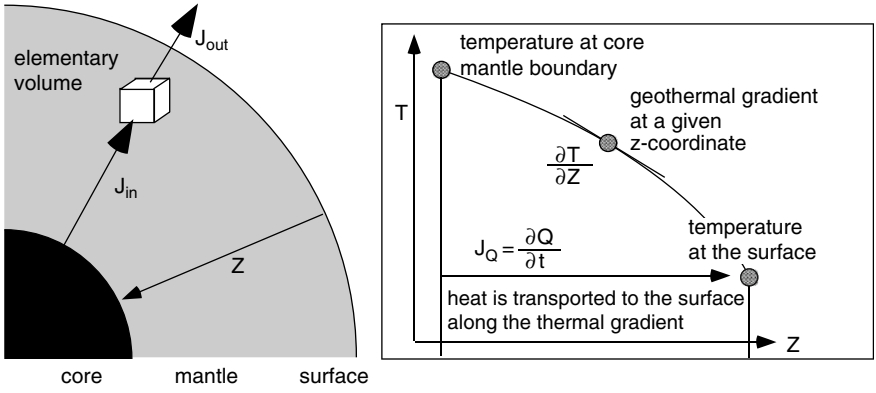

Fig. 3.5 Conductive heat transfer between hot interior and cold surface of the Earth

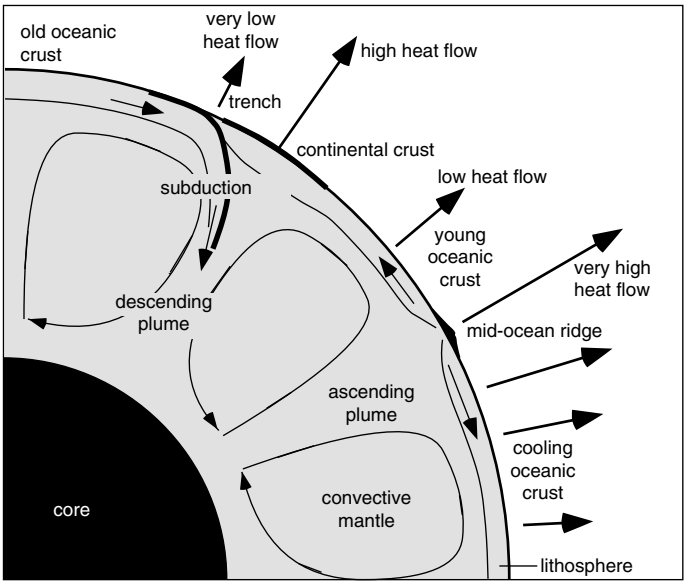

Fig. 3.6 Modification of steady-state heat flow resulting from conductive heat transfer by active tectonic processes. Heat flow at the surface varies by a factor of 4

The continental crust consists mostly of granitic rocks that produce about 30 mJ radioactive heat per kilogram and year. Oceanic crust, that is generally composed of basaltic rocks, produces about 5 mJ heat per kilogram and year, whereas mantle rocks produce only a small amount of radioactive heat (ca. 0.1 mJ heat per kilogram and year). The extra heat produced in the crust by decay of radioactive elements thus contributes significantly to the observed heat flow at the surface.

Heat flow through a specified volume of the crust may occur under the following conditions:

(a) Heat flow into the crustal volume is equal to the heat flow out from that volume. In this case the temperature in the volume remains constant. The temperature profile along thermal gradient z in Fig. 3.5 is independent of time (**steady-state geotherm**).
(b) Heat flow into the crustal volume is greater than the heat flow out from that volume. The excess heat put into the crustal volume will be used in two different ways. (1) to increase the temperature of the rock volume, (2) to drive endothermic chemical reactions in rocks.
(c) Heat flow into the crustal volume is lower than the heat flow out of the volume. In this case the heat loss of the volume of rock results in a temperature decrease (the rock cools). In this situation exothermic chemical reactions may produce extra heat to some extent. These reactions have the effect of preventing the rocks from cooling.

Different heat flow at the surface also has the consequence that rocks at the same depth in the crust and upper mantle may be at different temperatures leading to lateral heat transport parallel to the earth surface (parallel to xy-surfaces). An example is given in Fig. 3.7. Along a profile from Denmark to southern Norway the observed surface heat flows have been used by Balling (1985) to model the temperature field in the crust and mantle shown in Fig. 3.7. Because flow vectors are always normal to the force field from which the flow results, the heat flow trajectories will roughly look like the flow vectors shown in Fig. 3.7. It is obvious from this two dimensional section that at a given point in the crust the heat flow has a vertical **and** a horizontal component. Also note that the MOHO under the mid-Paleozoic continental crust of central Europe (Denmark) is at about 700 °C whereas the MOHO under the Precambrian crust of the Baltic Shield in the north is only at about 350 °C. It follows that the base of continental crust may be at largely different temperatures depending on the state and evolutionary history of a lithosphere segment and on the thermal regime deeper in the mantle. Observed surface heat flows can be translated into geotherms that may be time-dependent geotherms or steady-state geotherms. Such model geotherms are shown in Fig. 3.8 together with typical associated surface heat flows and temperatures at an average MOHO depth beneath continents of about 35 km (corresponding to about 1 GPa pressure). The geotherms represent curves that relate temperature with depth. The geothermal gradient (expressed as dT/dz) is the slope of the geotherm at a given depth in the crust or mantle and characterizes the temperature increase per or depth increment. In this book, you will see many *P–T* diagrams with *T* on the x-axis and *P* on the

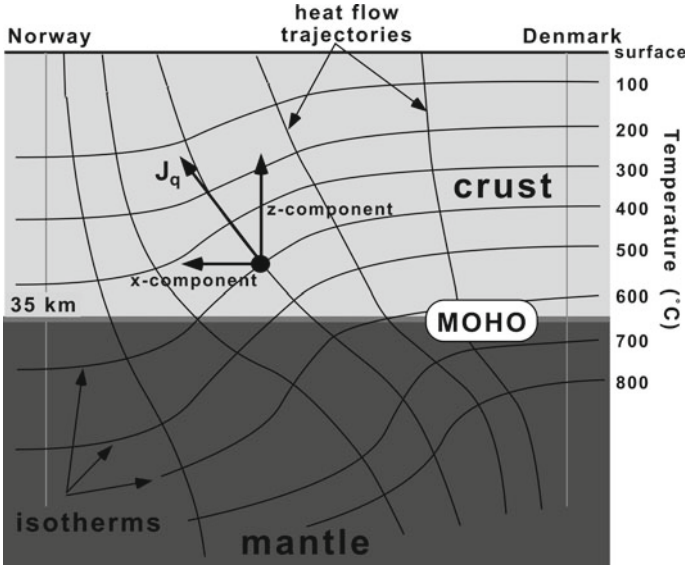

Fig. 3.7 Modeled temperature field along a cross section from Denmark to Norway (after Balling 1985)

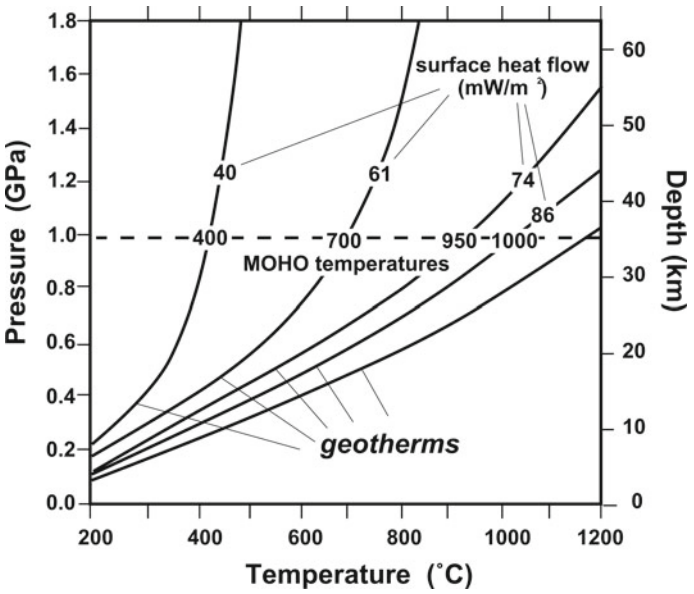

Fig. 3.8 Model geotherms with associated surface heat flow values and MOHO temperatures

y-axis. Pressure increases proportional with depth (for details see Sect. 3.2.4). Thus steep geotherms (or paths of metamorphism) on these figures correspond to low geothermal gradients, flat geotherms represent high geothermal gradients. Geotherms have high gradients near the surface and the gradients become progressively lower with increasing depth.

3.2.2.1 Transient Geotherms

Temperature changes in crust and mantle are caused by adding or removing extra heat to the rocks. Heat flow changes may have a number of geological causes. Deep-seated causes include changes in the relative positions of lithosphere plates and their continental rafts relative to mantle convection systems (Fig. 3.6). Collision of lithosphere plates may lead to subduction of oceanic crust and cause abnormal thermal regimes. Collision of continental rafts leads to extreme crustal thickening (from 35 km of normal continental thickness to 70 km in active collision zones, active example: Himalayas). Smaller volumes of crust can be moved relative to each other, for instance during a continent–continent collision. The formation of nappes and the stacking of slices of crust are typical examples of redistribution of rocks in crust and mantle. A very efficient way to transfer large amounts of heat to the crust is the transport by melts (magmatic heat transfer). Large volumes of mantle-derived basaltic melt may underplate continental areas and release enormous amounts of latent heat of fusion during solidification. Heat transported to the crust by upward migrating magma chambers locally disturbs the thermal regime and the temperature field in the crust.

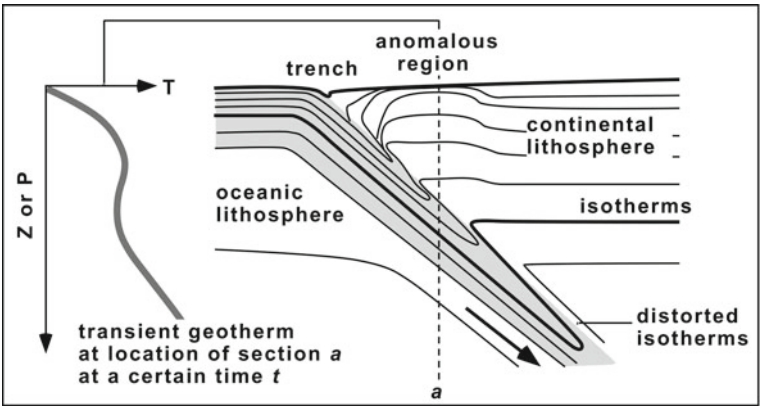

Fig. 3.9 Isotherm configuration within a cross section through an Andean-type subduction zone and a transient geotherm at location a (Peacock 1990)

Also, all tectonic transport modifies the pre-tectonic steady-state geotherm. At any one instant during active tectonics, the crust is characterized by a specific geotherm that relates temperature to depth. The geotherm is now changing with time. These **transient geotherms** describe the temperature-depth relationship at a given time and for a given geographic location (xy-coordinates). Some aspects of tectonic transport and its effect on the instantaneous geotherm are depicted in Fig. 3.9. The figure shows schematically the temperature field along a cross section through an Andean-type destructive margin. The down-going slab of oceanic lithosphere is relatively cold. Thermal relaxation is a slow process compared to plate movement. The continental lithosphere above the subducted oceanic plate is characterized by a complex, thermally anomalous region that results from magmatic heat transfer and from smaller scale deformation in the crust (nappes). The geotherm at location **a** at a given instant (instantaneous geotherm) in the active history of the subduction event may look like the geotherm shown at the left side of Fig. 3.9. Tectonic transport may even be fast enough to create temperature inversion in a transient geotherm. Such temperature inversions will, however, be a very short-lived phenomena and they will be eliminated rapidly if subduction ceases.

3.2.3 Temperature Changes and Metamorphic Reactions

If a crustal volume receives more heat than required to maintain a steady-state geotherm, the volume of rock will experience an increase in temperature and it will undergo **prograde metamorphism**. The heat capacity of the rock determines how much the temperature rises in relation to the heat added. Typical heat capacities for silicate rocks are on the order of 1 kJ per kg rock and °C. Suppose a quartzite layer in the crust receives 100 kJ per kg rock extra heat, this heat will increase the temperature of the quartzite by 100 °C. When heated, some rocks must adjust their

mineralogy by chemical reactions in order to maintain a state of minimized total Gibbs free energy (as explained in the sections above). These endothermic reactions will consume part of the heat added to the rock. Dehydration reactions occur typically during prograde metamorphism. The reactions replace hydrous minerals (such as zeolites, micas, chlorite, amphibole) by less hydrous or anhydrous minerals and release H_2O to a fluid phase. This fluid may or may not escape from the site of production. Such reactions are strongly endothermic and consume a large amount of heat (about 90 kJ per mole H_2O released from hydrous minerals). Noe consider a layer of mica schist in the crust containing about 1 mol H_2O per kg rock. A temperature increase of 100 °C (as in the quartzite layer) may result in complete destruction of the hydrous minerals in this rock, and a total of 190 kJ per kg of schist is required to obtain the same temperature increase (100 kJ for the temperature increase and 90 kJ for the reaction).

The heat effect of mineral reactions in rocks also influences the temperature–time relationship in a volume of reactive rock. The case is illustrated in Fig. 3.10 using the antigorite breakdown reaction Atg $\Rightarrow$ Fo + Tlc + H_2O reaction as an example (see field example Fig. 5.7a). Supply of excess heat (in addition to the steady state heat flow) will cause an increase in temperature until the equilibrium conditions (T_e) of the chemical reaction are reached. The heat input will then be used for running the reaction over a certain period of time and the temperature remains constant until one of the two reactant minerals (in this case Atg) is used up. After completion of the reaction, the temperature of the rock will continue to increase (Fig. 3.10a). The *T-t* path is analogous to heating water to its boiling point. The temperature of the water increases to the boiling temperature as heat is added to the water. During boiling the water temperature remains constant and the heat is used to drive the reaction (phase transition) liquid water $\Rightarrow$ steam. After all the water is boiled off, further addition of heat will increase the temperature of the steam. However, metamorphic reactions do not start running exactly at T_e but require a certain degree of overstepping ΔT of the equilibrium conditions T_e (Fig. 3.10b). The ΔT is related to the activation energy of the reaction, which functions as a kinetic barrier. Once the activation energy has been accumulated in the rock the reaction converts serpentine to olivine, talc and fluid.

If a crustal volume receives less heat than it requires to maintain a steady state geotherm, it will cool and the rocks will be potentially affected by **retrograde metamorphism**. During cooling, it may become necessary for the rock to change its mineralogical composition in order to maintain a state of minimum Gibbs free energy. In our example, for a rock consisting of Fo + Tlc, the reaction Fo + Tlc + H_2O $\Rightarrow$ Atg converts all Fo + Tlc into Atg (in the presence of an H_2O fluid) as the rock cools to T_e (Fig. 3.10a) under equilibrium conditions. The heat released by the reaction buffers the temperature to a constant value (T_e) until one of the three reactants has been used up and further cooling can take place. The situation is analogous to removing heat from water. The temperature will decrease until water begins to freeze. As long as both reactant (liquid water) and product (ice) are present in the system, the temperature is confined to the freezing temperature. After conversion of all water into ice the temperature will continue to fall if further heat is removed from the ice.

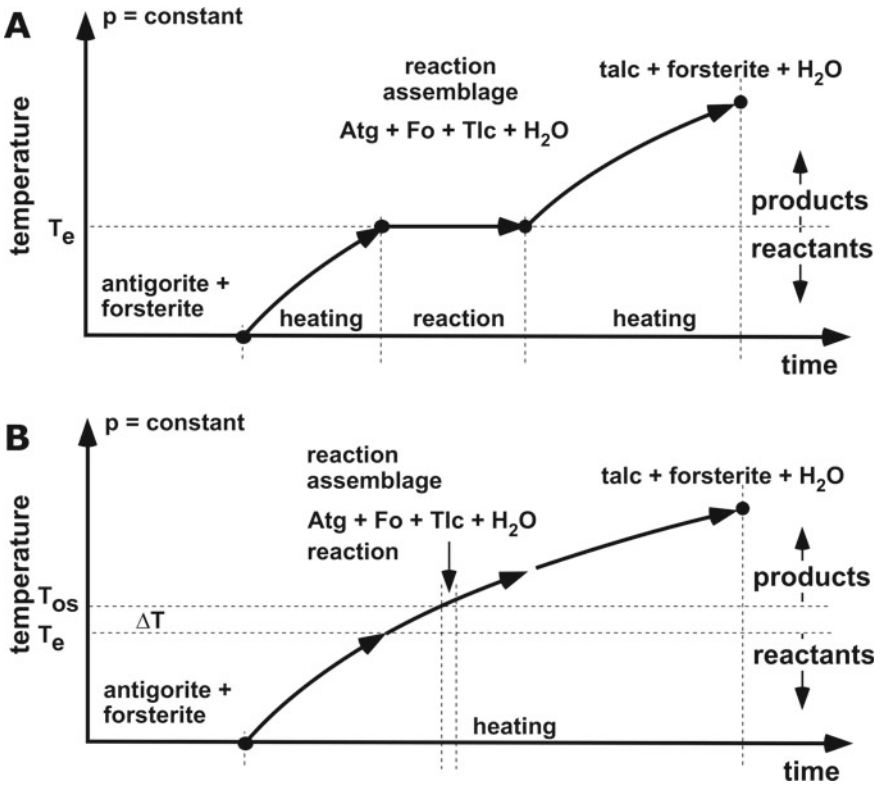

Fig. 3.10 Temperature vs. time diagrams for the reaction Atg = Fo + Tlc + H_2O during a period of increased heat flow: **a** Reaction sets in exactly at the equilibrium temperature T_e. *T* continues to increase after completion of the reaction. **b** Reaction sets in after a certain ΔT of overstepping at T_{OS}

3.2.4 Pressure Changes in Rocks

Normally, pressure in the crust and mantle is characterized by isobaric surfaces that are approximately parallel to the Earth's surface. As outlined above, the Gibbs free energy of minerals and associations of minerals (rocks) is also a function of pressure. Pressure changes in rocks are related to the change of position along the vertical space coordinate (z-axis in Fig. 3.5). The prevailing pressure at a given depth in a crustal profile with a steady-state geotherm is given by the density of the material above the volume of interest. It can be calculated from ($dP/dz = -g\rho$):

$$P_{(z)} = -g \int_0^z \rho_{(z)}\, dz + P_{(z=0)} \tag{3.10}$$

where g is the acceleration due to gravity (9.81 m s^{-2}), ρ is the density of the rock at any z (e.g. 2.7 g cm^{-3} = 2700 kg m^{-3}) and $P_{(z=0)}$ is the pressure at the surface (e.g. 10^5 Pa = 1 bar = 10^5 N m^{-2} = 10^5 kg m^{-1} s^{-2}). The z-axis direction is always taken as negative. With a constant, depth independent density, Eq. (3.10) reduces to the simple relationship P = g ρ z. The pressure, for example at 10 km (10 000 m) depth, is then calculated for an average rock density of 2700 kg m^{-3} as 265 MPa or 2.65 kbar. The pressure at the base of continental crust of normal thickness (35–40 km) is about 1 GPa. The pressure at z results from the weight of the rock column above the volume of interest and is designated as the **lithostatic pressure**. This pressure is usually nearly isotropic. Non-isotropic pressure (stress) may occur as a result of a number of geologically feasible processes and situations as discussed below.

A pressure difference of about 10 MPa at a depth of, e.g. 10 km (P ∼ 270 MPa) will occur if a column of nearby rocks has a different average density (e.g. 2800 instead of 2700 kg m^{-3}). If the density contrast of two columns of rock is 300 kg m^{-3} a ΔP of ∼9 MPa at a depth of 30 km is possible. This is nearly a 100 MPa at a total pressure of ∼0.8 GPa. However, because crustal material has similar densities, possible pressure differences between columns of rock at the same depth are limited to relatively small fractions of the lithostatic pressure (typically < 10%). However, such pressure gradients may cause flow of fluids stored in the interconnected pore space of rocks according to Darcy's law. The transport of fluids may cause chemical reactions in rocks through which the fluids pass if they are not in equilibrium with the solid assemblage of the rock.

Non-isotropic pressure (stress) also results from tectonic forces and from volume changes associated with temperature changes and composition changes of rocks and minerals. Stress is one of the major causes of the deformed structure of metamorphic rocks. It is also a very important force for small-scale migration and redistribution of chemical components. The processes of pressure solution, formation of fabric (such as foliation) and formation of metamorphic banding from homogeneous protolith rocks are caused by non-isotropic pressure distribution in rocks and associated transport phenomena (Figs. 2.3a, 2.4). The redistribution of material in stressed rocks attempts to reduce the non-isotropic pressure and to return to isotropic lithostatic pressure conditions.

There are two basic regimes how rocks respond by deformation to applied stresses. At high temperatures and lithostatic pressures rocks react by ductile deformation to stress, whereas brittle deformation is dominant at low-*T* and shallow depth. The two deformation regimes grade into one another at the brittle-ductile transition zone, which is located at about 12 km depth corresponding to about 318 MPa (3.2 kbar) pressure in typical anorogenic continental crust. The temperature at this depth is about 300 °C. The *P*–*T* conditions at the brittle-ductile transition zone correspond to those of the lower greenschist facies (see Chap. 4). The precise depth of the brittle-ductile transition depends on the amount of applied stress, the mechanical properties of the rocks (dependent on the type of rocks present) and the presence or absence of an aqueous fluid. In the brittle deformation regime rocks break and fracture in response to applied differential stress.

The created fractures fill normally with an aqueous fluid (liquid water) because the *P–T* conditions are in the field of liquid water (below the critical point of water, see Sect. 3.3). The fractures in crustal rocks above the brittle-ductile transition are typically well connected and form a permeable fracture network. The water in the fracture system is under hydrostatic pressure rather than lithostatic pressure conditions as described above. Thus hydrostatic pressure operating on water in a extension fracture at 10 km depth is about 100 MPa rather than the lithostatic 270 MPa as on the rock matrix on both sides of the fracture. Hydrothermal metamorphism, precipitation of fissure minerals, low-T rock alteration and similar processes occur typically under hydrostatic pressure conditions. Within the ductile deformation regime fluids tend to be close to lithostatic pressure.

In general, the lithostatic pressure acting on a volume of rock changes as a result of a change of depth of that rock volume (change of the position along the z-direction). In almost all geological occurrences, depth changes are caused by tectonic processes (that ultimately are also the result of thermal processes, e.g. mantle convection, density changes resulting from temperature changes). A lithosphere plate can be subducted in a collision zone and be transported to great depth in the mantle before it is resorbed by the mantle. Some of the subducted material may return to the surface before a normal steady-state geotherm is established. Metamorphic rocks of sedimentary or volcanic origin with mineral assemblages that formed at pressures in excess of 3.0 GPa have been reported from various orogenic belts; 3.0 GPa pressure is equivalent to about 100 km subduction depth ($z = -P/(g\rho)$). In continental collision zones the continental crust often is thickened to double its normal pre-collision thickness. At the base of the thickened crust the pressure increases from 0.9 to 1.8 GPa The conversion of the mineral assemblages of the rocks undergoing such dramatic pressure changes depend on the nature and composition of these rocks and will be discussed in Part II of the book.

Differential stresses acting on rocks may potentially be sufficiently large that they may trigger changes in the mineral assemblage. Differential stresses operate on various scales ranging from plate tectonic dimension to stresses along grain contacts in metamorphic rocks. The later stresses are related to dissimilar volume adjustments of different minerals during changing *P–T* and to local stresses caused by growth of new minerals and dissolution of reactant minerals during metamorphic reactions. Particularly vulnerable to stress effects are simple phase transitions such as quartz–coesite, coesite–stishovite, calcite–aragonite for example. Therefore, the pressure making these transitions possible can be composed of the lithostatic pressure plus the differential stress (e.g. Richter et al. 2016). This has the consequence that the total pressure cannot be directly converted to a depth below surface for the observed assemblage in the rock.

Variations in depth and associated pressure changes also can be related to subsiding sedimentary basins where a given layer **a** of sediment is successively overlain and buried by new layers **b, c** … of sediments. Layer **a** experiences a progressive increase in pressure and temperature. If sedimentation and subsidence is slow, layer **a** may follow a steady state geotherm. Metamorphism experienced by layer **a** is commonly described under the collective term **burial metamorphism** as

defined in Sect. 1.2.3. Crustal extension or lithosphere thinning is often the cause for the required subsidence creating deep sedimentary basins. Burial metamorphism is therefore also caused by tectonic processes.

3.3 Gases and Fluids

Sedimentary rocks such as shales often contain large modal proportions of hydrous minerals. In fact, sediments deposited in marine environments can be expected to contain, under equilibrium conditions, a mineral association that corresponds to a **maximum hydrated state**. Adding heat to the hydrous minerals (clays) of a sediment during a metamorphic event will drive reactions of the general form:

$$\text{hydrous assemblage} \Rightarrow \text{less hydrous or anhydrous assemblage} + H_2O \quad (3.11)$$

The general reaction (3.11) describes the dehydration process taking place during prograde metamorphism. The important feature of dehydration reactions is the release of H_2O. Steam is, in contrast to solid minerals, a very compressible phase and its volume is strongly dependent on pressure and temperature. In Fig. 3.11, the molar volume of H_2O is shown as a function of pressure and temperature. At low temperatures, H_2O occurs either as a high density liquid phase or as a low density steam phase depending on the prevailing pressure. The phase boundary between liquid and steam H_2O is the boiling curve. With increasing temperature the density contrast between steam and liquid H_2O continuously decreases along the boiling curve. At the critical point, steam and liquid have the same density and the distinction between steam and liquid becomes redundant. At temperatures above the critical point the H_2O phase is therefore a **supercritical fluid phase** or simply a fluid. Water in metamorphic systems at temperatures above 374 °C is referred to as an (aqueous) **fluid phase** or a **fluid**. The critical point of H_2O is at 374 °C and 21.77 MPa.

Metamorphic fluids usually predominantly consist of H_2O. The H_2O of aqueous fluids in metamorphic rocks has its origin from various sources: (1) relic formation waters of sedimentary rocks, (2) dehydration water from H_2O originally stored in hydrous minerals, (3) meteoric water, and (4) magmatic water released from solidifying magmas. In the lower crust and in crustal segments with abundant carbonate rocks, CO_2 may become an additional important component in the fluid phase. Aqueous fluids also may contain significant amounts of dissolved salts (NaCl) and other solutes (e.g. aqueous silica complexes). At temperatures below 265 °C (at 200 MPa), H_2O and CO_2 mixtures form two separate phases. At higher temperatures, H_2O and CO_2 form continuous solutions ranging from pure H_2O to pure CO_2. However, extremely NaCl-rich brines may unmix into a dense aqueous brine and a low density CO_2-rich vapor phase even under fairly high metamorphic *P–T* conditions. The composition of the most common binary metamorphic CO_2-H_2O fluids is normally reported in terms of mole fraction X_{H_2O} (or X_{CO_2}). The

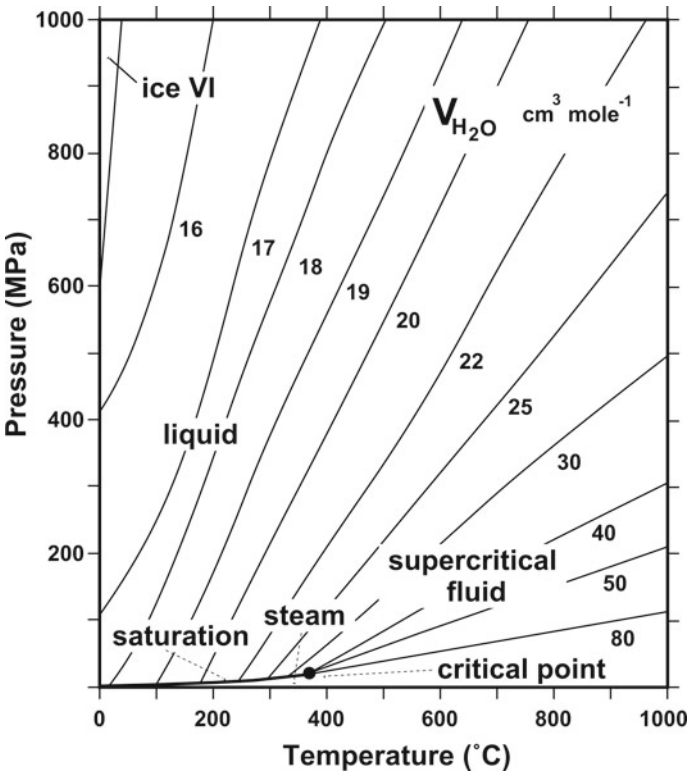

Fig. 3.11 Isochores of H_2O as a function of pressure and temperature (Helgeson and Kirkham 1974)

dimensionless quantity X_{H_2O} is the ratio of the number of moles of H_2O and the total number of moles of H_2O and CO_2 in the fluid phase $X_{H_2O} = n_{H_2O}/(n_{H_2O} + n_{CO_2})$. An X_{H_2O} of 0.5 indicates, for example, a fluid with equal amounts of H_2O and CO_2 on a mole basis. Other molecular gas species found in metamorphic fluids include: CH_4, N_2, HCl, HF, and many others.

The low density fluid produced during prograde dehydration is transported away from the site of production through interconnected pore space and lost to the system. If the rate of H_2O production exceeds the rate of transport, then the local pore pressure increases. However, the fluid pressure that may build up this way does not greatly exceed the lithostatic pressure imposed on the solid rock, but if the mechanical strength of the rocks is exceeded, then failure occurs. This mechanism of **hydraulic fracturing** produces the necessary transport structure for dehydration water. The fluid released is quickly transported and channelled away from the area undergoing dehydration. Suppose a rock undergoes dehydration at 0.5 GPa and 600 °C. The produced fluid (Fig. 3.11) has a molar volume of about 22 cm^3 that corresponds to a density of about 0.82 g cm^{-3}. This is a remarkably high density

for H_2O at 600 °C but it is still much lower than the typical density of rock-forming minerals of about 3 ± 0.5 g cm^{-3}. The large density contrast between fluid and solids results in strong buoyancy forces and a rapid escape of the fluid from the rocks. Most metamorphic rocks are probably free of fluid during periods without reaction with the exception of fluids trapped in isolated pore spaces, as thin films along grain boundaries, and as inclusions in minerals (**fluid inclusions**).

In most cases, the bulk composition of a metamorphic rock determines the mineral assemblage present at any point on a prograde *P–T* path. In turn, the mineral assemblage will control (buffer) the composition path followed by the fluid. Thus, in most metamorphic rocks the fluid composition is internally controlled.

3.4 Time Scale of Metamorphism

Some simple considerations allow for an estimate of the time scale of typical orogenic metamorphism (see also Walther and Orville 1982). The range of reasonable heat flow differences in the crust that can drive metamorphic processes is constrained by maximum heat flow differences observed at the surface. The highest heat flows are measured along mid-ocean ridges (120 mW m^{-2}), whilst the lowest are in old continental cratons (30 mW m^{-2}). Consider a crustal layer with a heat flow difference between bottom (75 mW m^{-2}) and top (35 mW m^{-2}) of 40 mW m^{-2}. This means that every second the rock column receives 0.04 J heat (per m^2). If the layer consists of shales (heat capacity = 1 kJ kg^{-1} $°C^{-1}$) with a volatile content (H_2O and CO_2) of about 2 mol kg^{-1}, the heat received will be used to increase the temperature of the rock and to drive endothermic devolatilization reactions. About 90 kJ heat are required to release 1 mol H_2O or CO_2. If complete devolatilization occurs in the temperature interval 400–600 °C, a total of 380 kJ will be consumed by the shale (180 kJ for the reactions and 200 kJ for the temperature increase from 400 to 600 °C). It takes 9.5 × 10^6 s (0.3 years) to supply 1 kg of rock with the necessary energy. Using a density of 2.63 g cm^{-3}, 1 kg of rock occupies a volume of 380 cm^3 and it represents a column of 0.38 mm height and 1 m^2 ground surface. From this it follows that metamorphism requires about 8 years to advance by 1 cm. Eight million years (Ma) are required to metamorphose a 10 km thick layer of shale. Similarly, if the heat flow difference is only 20 mW m^{-2}, and the shale layer is 20 km thick layer with an initial temperature 200 °C, it will require about 48 Ma of metamorphism to convert the hydrous 200 °C shale to an anhydrous 600 °C metapelitic gneiss.

These crude calculation shows that typical time spans for regional scale metamorphic processes are on the order of 10 to 50 million years. Similar time scales have been derived from radiometric age determinations.

3.5 Pressure–Temperature-Time Paths and Reaction History

During tectonic transport, any given volume of rock follows its individual and unique path in space and time. Each volume of rock may experience loss or gain of heat, and changes of its position along the z-coordinate result in changes in lithostatic pressure loaded on the rock. Figure 3.12 shows again a simple model of a destructive plate margin. The situation here depicts a continent–continent collision with the formation of continental crust twice its normal thickness. In A at t_1 (0 Ma) there is a volume of rock (a rock unit indicated by an open square) at depth **c**, the position of which changes depth with time (t_1 through to t_6 at 30 Ma). In B through E, the position of the rock unit (filled squares) during tectonic transport is shown in terms of *P–T* space. The time slices are arbitrary and have been chosen in accordance with time scales of the formation of Alpine-type orogenic belts. At t_1 the rock unit lies on a stable steady-state geotherm. At t_2 (10 Ma) tectonic transport moves the crust together with the rock unit beneath another continental crust of normal 35 km thickness. Increasing depth of the rock unit is accompanied by increasing pressure (Eq. 3.10). At the same time, the rock unit begins to receive more heat than at its former position at t_1. However, because heat transport is a slow process compared with tectonic transport, dP/dT tends to be much steeper (C) than the corresponding

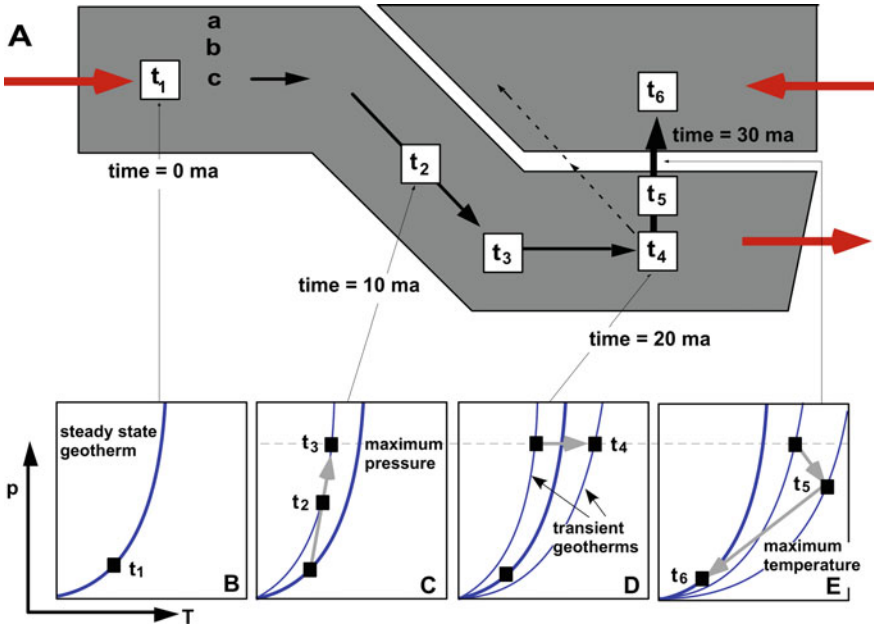

Fig. 3.12 Schematic diagram showing the position of a rock unit in the crust as a function of time during continent–continent collision and the corresponding paths followed by the rock unit in *P–T* space

dP/dT slope of the initial steady-state geotherm (B). Between t_1 and t_2, the rock unit has traveled in *P–T* space along a path that is on the high-pressure side of the initial steady-state geotherm. The rock unit is now on a transient geotherm that changes its shape as time progresses. At t_3 the crust is twice its normal thickness (about 70 km), which is about the maximum thickness in continent–continent collision zones. The rocks have reached their maximum depth and consequently their maximum pressure of about 2 GPa (C). Continued plate motion does not increase the thickness of the crust and pressure remains constant as long as underthrusting is going on. On the other hand, heat transfer to the rock unit in question increases the temperature as shown in D (t_4). From this time, a number of feasible mechanisms may control the path of the rock unit. Continued tectonic transport may return slices and fragments of rock to shallower levels in a material counter current (dashed arrow in A), or simply, after some period of time, plate convergence stops, e.g. because frictional forces balance the force moving the plate. The thickened crust starts to uplift, and erosion restores the crust to its original thickness. By this mechanism the rock unit may return to its original depth position and, given enough time, the stable steady-state geotherm will be re-established. The path between t_4 and t_5 is characterized by decompression (transport along the z-axis). If initial uplift rates are slow compared with heat transport rates, the rocks will experience a continued temperature increase during uplift as shown in E). However, at some stage along the path the rocks must start to lose more heat to the surface than they receive from below, and consequently cooling begins. The point t_5 in E represents the maximum temperature position of the path traveled by the rock unit. At t_6 the rock has returned to its former position on the steady state geotherm (A).

The consequences for pressure and temperature of the geologic process illustrated in Fig. 3.12 are summarized in Fig. 3.13. A rock at depth ***c*** (*P–T–t* path 3) follows a clockwise pressure–temperature loop. Such clockwise *P–T–t* paths are a characteristic feature of orogenic metamorphism and have been documented from such diverse mountain belts as the Scandinavian Caledonides, western Alps, Appalachians, and Himalayas. In detail, clockwise *P–T–t* loops may show a number of additional complications and local features. Counter-clockwise *P–T–t* paths have been reported from granulite facies terrains where an event of heating from igneous intrusions precedes crustal thickening. They may also occur in terrains that have experienced an initial phase of crustal extension. Very often "normal" orogenesis, is characterized by the following sequence of *P–T–t* path sections: isothermal thickening, isobaric heating, isothermal decompression and isobaric cooling. Returning to Fig. 3.13a, it is evident that the maximum temperature point along the *P–T–t* path followed by a metamorphic rock does not necessarily coincide with the maximum pressure point of the path. This means that maximum pressure and maximum temperature will be generally diachronous.

What do we see of the path traveled by a rock in *P–T–t* space when we study a metamorphic rock? If the rock has always maintained an equilibrium state and metamorphism is strictly isochemical, we will not find any relics of its metamorphic history. However, rocks that formed at, for example, 800 °C and 1.0 GPa can be collected at the surface and they ***do*** show characteristic high-*P–T* mineral

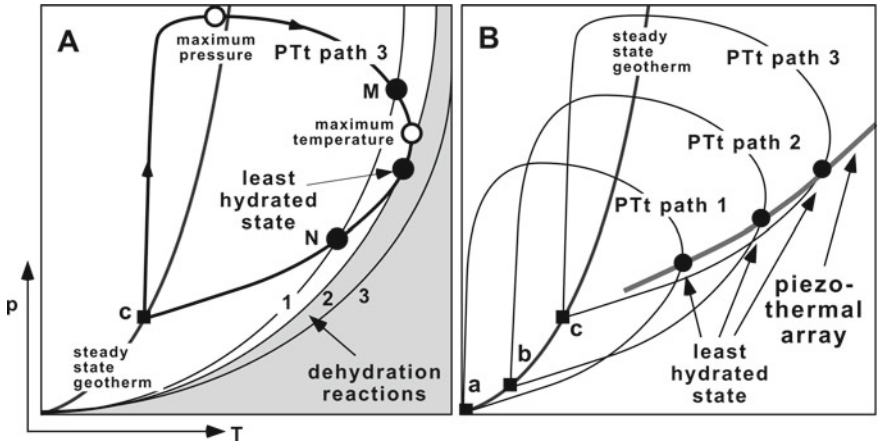

Fig. 3.13 **A** *P–T-t* path of a rock unit starting from point c at t = 0. The mineral assemblage stable at the tangent point of the path with a dehydration reaction 2 will, in general, be preserved in metamorphic rocks. The tangent point corresponds to the least hydrated state of the rock. **B** Clockwise *P–T-t* loops for three crustal rock units from different depth levels (a, b and c). The mineral assemblage found in samples from the individual rock units corresponds to the least hydrated state. The *P–T* points of the least hydrated state from all rocks of a metamorphic terrain define a curve that is known as a piezo-thermal array (∼metamorphic field gradient)

assemblages! This immediately tells us that at some stage during the reaction history a certain high-grade mineral assemblage has not been converted to low-grade assemblages on the way back to the surface. The question is: which point (or points) along the *P–T* path is preserved and recorded by the mineral assemblage (s) of the rock? The answer may be difficult to find in a specific geologic situation and for specific samples. However, low-grade rocks e.g., shale, often contain modally large amounts of hydrates and are, therefore, affected by a series of discontinuous and continuous dehydration reactions during prograde metamorphism. In the pressure–temperature range typical for crustal metamorphism, dehydration reactions have equilibrium conditions as shown in Fig. 3.13a (reactions 1, 2 and 3). Path 3 will be shaped by dehydration reactions and when crossing dehydration reaction 1 at point **M** a rock will partially lose water and continue as a rock containing a smaller amount of hydrous minerals (mica, chlorite, amphibole). Dehydration of the rock will continue until the tangent point of the *P–T* path where the last active dehydration reaction is reached. This point corresponds to the **least hydrated state** in the metamorphic history of the rock. It does not necessarily correspond to the maximum temperature point reached by the rock. If the *P–T–t* path shows a pronounced period of rapid uplift and decompression, the *P–T* coordinates of the least hydrated state may be dramatically different from maximum *P* and *T*. At this point the rock contains a prograde assemblage in equilibrium with an aqueous fluid phase saturating the mineral grain boundaries and filling the pore space. However, the total amount of free fluid is extremely small in most

metamorphic rocks. Typical flow porosities of metamorphic rocks at P and T are on the order of 0.2 vol% (e.g. 2 cm^3 H_2O/1000 cm^3 rock). After having passed the point of the least hydrated state, the rock crosses the dehydration reactions in the reversed direction. The reactions consume water and form hydrates from anhydrous (or less hydrous) minerals and the minute amount of free fluid will be readily used up by the first rehydration reaction. For example, 2 ‰ free H_2O in a rock of an appropriate composition and mineral assemblage at 0.9 GPa and 700 °C (corresponding to 0.1 mol H_2O per 1000 cm^3 of rock) can be used to form 15 cm^3 biotite per 1000 cm^3 rock (1.5 vol. % biotite). The rock will then be devoid of a free fluid phase which effectively prevents its minerals adjusting to changing P–T conditions. This is because water is not only essential in dehydration reactions but plays a central role as a transport medium and catalyst for chemical reactions in rocks. Its final loss marks the closure the reaction history of a rock. Even reconstructive phase transitions, e.g. kyanite = sillimanite, require the presence of water in order to proceed at finite rates even over geological time scales. Consequently, by studying the phase relationships of metamorphic rocks, one will in general only be able to determine the P–T conditions corresponding to the least hydrated state. This is close to the conditions when a free aqueous fluid was last present in the rock.

On its way to the surface the rock crosses reaction 1 at point N (Fig. 3.13a). However, the reaction will affect the rock only if water is available for the back reaction. Rehydration (retrograde metamorphism) is widespread and very common in metamorphic rocks. However, rehydration reactions very often do not run to completion, and assemblages from the least hydrated state more often than not survive as relics. The necessary water for retrograde metamorphism is usually introduced to the rocks by late deformation events. Deformation may occur along discrete shear and fracture zones that also act as fluid conduits. The shear zone rocks may contain low-grade mineral assemblages whereas the rocks unaffected by late deformation still show the high-grade assemblage. With some luck, it is possible to identify in a single rock sample a series of mineral assemblages that formed at consecutive stages of the reaction history. The reaction history of rocks can often be well documented for all stages that modified the assemblage of the least hydrated state.

Relics from earlier portions of the P–T path (before it reached its least hydrated state) are seldom preserved in metasedimentary rocks. Occasionally, early minerals survive as isolated inclusions in refractory minerals such as garnet. Garnet in such cases effectively shields and protects the early mineral from reacting with minerals in the matrix of the rock with which it is not stable at some later stage of the rock's history. Rocks with water-deficient protoliths such as basalts, gabbros and other igneous rocks may better preserve early stages of the reaction history. In some reported case studies, meta-igneous rocks record the entire P–T–t path from the igneous stage to subduction metamorphism and subsequent modifications at shallower crustal levels (see Sect. 9.8.2.1).

Rocks collected in a metamorphic terrain may originate from different depth levels in the crust (Fig. 3.12, depths a, b, and c). All rocks follow their individual P–T path as indicated in Fig. 3.13b. Analysis of phase relationships and geologic

thermobarometry may therefore yield a series of different *P–T* coordinates corresponding to the least hydrated states of the individual samples. The collection of all *P–T* points from a given metamorphic terrain define a so-called **piezo-thermic array**. Its slope and shape characterize the specific terrain. The details of a piezo-thermic array of a given terrain depend on the geologic history and dynamic evolution of the area. The term "**metamorphic field gradient**" is preferred by some petrologists over the expression piezo-thermic array, but both expressions mean essentially the same thing. It is an arrangement of *P–T*-points of least-hydrated state conditions reached during a now **fossil** metamorphism by rocks that are exposed **today** on the erosion surface of the planet. It is important to note that this two-dimensional array of *P–T* points should ***not*** be confused with a geotherm.

3.6 Chemical Reactions in Metamorphic Rocks

Chemical reactions in rocks may be classified according to a number of different criteria. Below follows a brief presentation of various kinds of reactions that modify the mineral assemblage or the mineral composition of metamorphic rocks.

3.6.1 Reactions Among Solid-Phase Components

These are often termed "solid–solid" reactions because only phase components of solid phases occur in the reaction equation. Typical "solid–solid" reactions are, for example:

3.6.1.1 Phase Transitions, Polymorphic Reactions

Al_2SiO_5	Ky = And; Ky = Sil; Sil = And
$CaCO_3$	calcite = aragonite
C	graphite = diamond
SiO_2	α-Qtz = β-Qtz; α-Qtz = coesite, ……
$KAlSi_3O_8$	microcline = sanidine

3.6.1.2 Net-Transfer Reactions

Such reactions transfer the components of reactant minerals to minerals of the product assemblage.

Reactions involving anhydrous phase components only

$$\mathrm{Jd} + \mathrm{Qtz} = \mathrm{Ab}$$

$$\mathrm{Grs} + \mathrm{Qtz} = \mathrm{An} + 2\ \mathrm{Wo}$$

$$2\ \mathrm{Alm} + 4\ \mathrm{Sil} + 5\ \mathrm{Qtz} = 3\ \mathrm{Fe\text{-}Crd}$$

Volatile-conserving "solid–solid" reactions

$$\mathrm{Tlc} + 4\ \mathrm{En} = \mathrm{Ath}$$
$$\mathrm{Lws} + 2\ \mathrm{Qtz} = \mathrm{Wa}$$
$$2\ \mathrm{Phl} + 8\ \mathrm{Sil} + 7\ \mathrm{Qtz} = 2\ \mathrm{Ms} + \mathrm{Crd}$$

3.6.1.3 Exchange Reactions

These reactions exchange components between a set of minerals.

Reactions involving anhydrous phase components only

Fe–Mg exchange between olivine and orthopyroxene: Fo + Fs = Fa + En
Fe–Mg exchange between clinopyroxene and garnet: Di + Alm = Hed + Prp

Volatile-conserving "solid–solid" reactions

Fe–Mg exchange between garnet and biotite: Prp + Ann = Alm + Phl
Cl-OH exchange between amphibole and biotite: Cl-Fpa + OH-Ann = OH-Fpa + Cl-Ann

3.6.1.4 Exsolution Reactions/Solvus Reactions

High-T alkali feldspar = K-feldspar + Na-feldspar
Ternary high-T feldspar = meso-perthite + plagioclase
Mg-rich calcite = calcite + dolomite
High-T Cpx = diopside + enstatite
Al-rich Opx = enstatite + garnet

The common feature of all "solid–solid" reactions is that equilibrium conditions of the reaction are independent of the fluid phase composition, or more generally speaking, of the chemical potentials of volatile phase components during metamorphism. It is for this reason that all "solid–solid" reactions are potentially useful geologic thermometers and barometers. The absence of volatile components in the reaction equation of "solid–solid" reactions should not be confused with general fluid-absent conditions during reaction progress. Metamorphic reactions generally require the presence of an aqueous fluid phase in order to achieve significant reaction progress even in geological time spans, attainment of chemical equilibrium in larger scale domains and chemical communication over several grain-size dimensions. Although *P*–*T* coordinates of the simple reconstructive phase transition kyanite = sillimanite are independent of μ_{H_2O}, , the detailed reaction mechanism may involve dissolution of kyanite in a saline aqueous fluid and precipitation of sillimanite from the fluid at nucleation sites that can be structurally unrelated to the former kyanite (e.g. Carmichael 1968). It is clear that the chlorine-hydroxyl

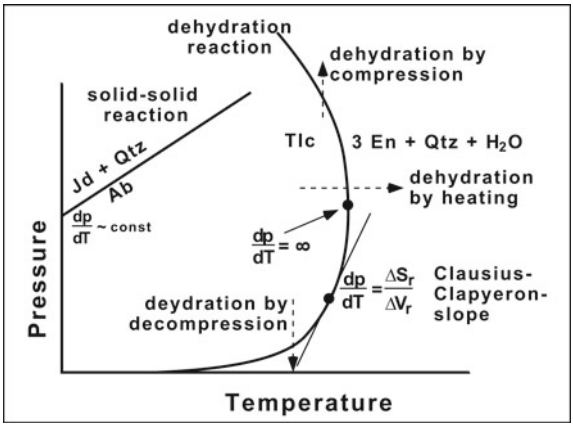

Fig. 3.14 Schematic equilibrium conditions of solid–solid and dehydration reactions in *P–T* space and the Clausius–Clapeyron equation (ΔS_r = entropy change and ΔV_r = volume change of the reaction)

exchange between amphibole and mica represents a process that requires the presence of an saline aqueous fluid. However, the equilibrium of the exchange reaction is independent on the composition of that fluid.

Phase transitions, "solid–solid" net transfer and exchange reactions often show straight line equilibrium relationships in *P–T* space. The slope of the equilibrium line of such reactions can be readily calculated (estimated) from the Clausius–Clapeyron equation (Fig. 3.14).

3.6.2 Reactions Involving Volatiles as Reacting Species

3.6.2.1 Dehydration Reactions

Reactions involving H_2O are the most important metamorphic reactions. Low-grade metasediments contain modally abundant hydrous minerals. Pelitic rocks consist mainly of clay minerals (and zeolites) at low-grade. Serpentine minerals make up lower-grade ultramafic rocks. These sheet silicates contain up to about 12 wt. % H_2O. The hydrous minerals are successively removed from the rocks by continuous and discontinuous dehydration reactions as heat is added to them. Release of H_2O during prograde metamorphism of H_2O-rich protoliths ensures that a free H_2O fluid is present in the rocks either permanently or periodically during the progress of dehydration reactions. This in turn often permits discussion of metamorphism for conditions where the lithostatic pressure acting on the solids also applies to a free fluid phase. If the fluid is pure H_2O (and choosing an appropriate standard state), the condition is equivalent to $a_{H_2O} = 1$. The general shape of dehydration equilibria is shown schematically in Fig. 3.14. Using the talc breakdown reaction as an example, the general curve shape of dehydration reactions on *P–T* diagrams can be deduced as follows:

$$\text{Tlc} = 3\ \text{En} + 1\ \text{Qtz} + 1\ \text{H}_2\text{O}\ (\text{V}) \tag{3.12}$$

The dP/dT-slope of a tangent to the equilibrium curve is given at any point along the curve by the Clapeyron equation. All dehydration reactions have a positive ΔS_r (entropy change of reaction) and the curvature is largely controlled by the volume change of the reaction. The volume term can be separated into a contribution from the solids and the volume of H_2O, respectively:

$$\Delta V_r = \Delta V_{solids} + \Delta V_{H_2O} \tag{3.13}$$

The volume change of the solids can be calculated from:

$$\Delta V_{solids} = 3\ V_{En} + 1\ V_{Qtz} - 1\ V_{tlc} \tag{3.14}$$

ΔV_{solids} is a small and negative quantity and varies very little with P and T. Consequently, the curve shape of dehydration reactions largely reflects the volume function of H_2O, that is shown in Fig. 3.11. At low pressures, V_{H_2O} is large and the dP/dT-slope small. In the pressure range of about 200–300 MPa, the molar volume of H_2O rapidly decreases and dehydration reactions tend to be strongly curved. At pressures greater than about 300 MPa and up to 1.0–1.5 GPa, the volume of H_2O is usually comparable to the volume change of the solids and ΔV_r tends to be very small. Perceptively, dP/dT slopes are very large in this pressure range. At even higher pressures, the volume of H_2O cannot compensate the negative ΔV_{solids} and ΔV_r and the dP/dT-slope also become negative. From the general shape of dehydration equilibria in *P–T* space shown in Fig. 3.14, it is evident that talc, for instance, can be dehydrated either by heating, by decompression or by compression.

The dehydration of zeolite minerals is often accompanied by large negative ΔV_{solids} and the dehydration equilibria have negative slopes already at moderate or low pressures. For example, the reaction analcime + quartz ⇒ albite + H_2O has a ΔV_{solids} of -20.1 cm^3 $mole^{-1}$ and the equilibrium has a negative slope above pressures of about 200 MPa.

In contrast to dehydration reactions, dP/dT-slopes of "solid–solid" reactions (and phase transitions) are nearly constant (Fig. 3.14).

The equilibrium constant of the talc breakdown reaction [3.12] can be expressed by the mass action equation:

$$K = \frac{a_{En}^3 a_{Qtz} a_{H_2O}}{a_{Tlc}} \tag{3.15}$$

where a_i denotes the activity of the subscripted phase component. The activity of a phase component is a function of the composition of the phase. Its numerical value also depends on the choice of a standard state, explicitly the conditions where the activity shall be equal to one. The equilibrium constant K of a chemical reaction has a fixed value at a given *P* and *T* (a constant as the name suggests). It can be calculated from the fundamental equation that is also extremely useful for geological applications:

$$-\mathrm{R\ T\ ln\,K} = \Delta G_r^{\circ} \tag{3.16}$$

The standard state Gibbs free energy change of the reaction on the right hand side of Eq. (3.16) can be calculated for P and T of interest provided the thermodynamic data for all phase components in the reaction are known (R = universal gas constant; T = temperature in K). For the talc reaction Eq. (3.12) the logarithmic form of Eqs. (3.15) and (3.16) is:

$$\ln K = \left\{\ln a_{H_2O} + \left[\ln a_{En}^3 + \ln a_{Qtz} - \ln a_{Tlc}\right]\right\} = -\Delta G_r^{o}/(\mathrm{R\ T}) \tag{3.17}$$

With the appropriate standard state and by considering pure end member solids i (a_i = 1), the expression in square brackets becomes zero and the equilibrium is dependent on the activity of H_2O. The equilibrium is shown in Fig. 3.14 for the case $P_{H_2O} = P_{lithostatic}$ (pure H_2O fluid present, $a_{H_2O} = 1$). Equation (3.16) is graphically represented in Fig. 3.15 for three values of a_{H_2O}. It can be seen from Fig. 3.15, that the equilibrium conditions for dehydration reactions are displaced to lower temperatures (at P = constant) by decreasing a_{H_2O}. Solutions of Eq. (3.17) for different a_{H_2O} are also shown in Fig. 3.16. It follows from Fig. 3.16 that the maximum temperature for the talc-breakdown reaction is given by the condition $a_{H_2O} = 1$ that is equivalent to $P_{H_2O} = P_{lithostatic}$ and the presence of a pure H_2O fluid.

It also follows from Fig. 3.16, that talc dehydrates to enstatite and quartz at lower temperatures if $a_{H_2O} < 1.0$ at any pressure. The *P–T* space can, therefore, be contoured with a series of dehydration curves of constant a_{H_2O}. Geologically, the condition of $a_{H_2O} < 1.0$ can be realized basically in two different situations: (1) the fluid is not a pure H_2O fluid but is rather a mixture of H_2O and some other components not taking part in the reaction (e.g. CH_4, N_2, CO_2), (2) there is no free fluid phase present at all.

The equilibrium curve for the condition $P_{H_2O} = P_{hydrostatic}$ has a shape similar to the $P_{H_2O} = P_{lithostatic}$ curve. The two curves converge at very low pressures. Note, however, that here $a_{H_2O} = 1$ along the curve (standard state: pure H_2O at T and

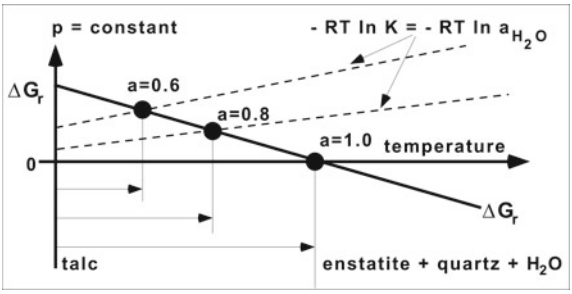

Fig. 3.15 Solutions of the equation $\Delta G_r^{\circ} = -\mathrm{RT\ ln\,K}$ for dehydration reactions (here the talc-breakdown reaction) and three different values of a_{H2O}

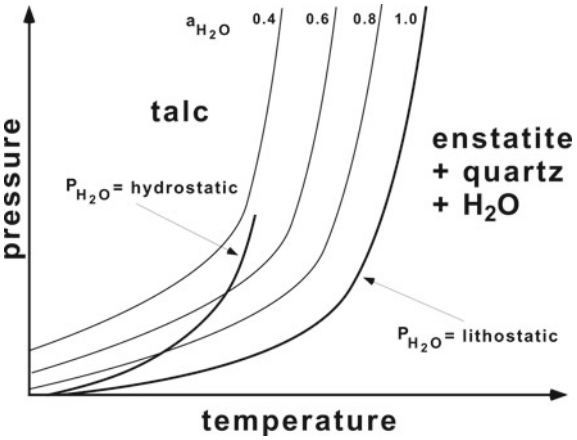

Fig. 3.16 Schematic equilibrium conditions of dehydration reactions (here the talc-breakdown reaction) for various a_{H_2O} conditions

$P_{hydrostatic}$), and that it does not vary with increasing pressure. Also note that under the condition $P_{H_2O} = P_{hydrostatic}$, the pressure is different for the solids and the fluid. This means that such a system is not in mechanical equilibrium. Hydrostatic pressure conditions may occur in very porous or strongly fractured rocks at shallow crustal levels. Typical geologic settings where such conditions may occur include hydrothermal vein formation, oceanic metamorphism, shallow level contact aureoles, and deep groundwater in basement rocks. Hydrostatic pressures usually cannot be maintained at typical metamorphic pressures of several hundred MPa. Pressure solution and local chemical redistribution of material rapidly isolates the fluid phase and the system returns to mechanical equilibrium. Geologically then, the situation $P_{H_2O} = P_{lithostatic}$ is the most important one and the curves $a_{H_2O} < 1$ may be relevant in rocks with an impure aqueous fluid or in "dry" environments.

3.6.2.2 Decarbonation Reactions

This type of reaction describes the decomposition of carbonate minerals such as calcite and dolomite. For example, adding heat to a rock containing calcite and quartz will eventually cause the following reaction: Cal + Qtz = Wo + CO_2 (Fig. 3.17). The form of the equilibrium conditions in *P–T* space is analogous to the dehydration reactions depicted in Fig. 3.16 as are the effects of variations in a_{CO_2} (P_{CO_2}). The highest temperature of the reaction at any pressure occurs where $a_{CO_2} = 1$. In metamorphosed carbonate rocks, the fluid phase rarely consists of pure CO_2, and is usually a mixture of CO_2 and H_2O (and other volatile species).

3.6.2.3 Mixed Volatile Reactions

In rocks containing both, hydrous minerals (sheet silicates and amphiboles) and carbonates, reactions may produce or consume both CO_2 and H_2O simultaneously. In such rock types the fluid phase contains at least the two volatile species, CO_2 and H_2O. Under certain conditions, for instance where graphite is present, other species such as H_2 and CH_4 may be occur in the fluid phase in significant amounts.

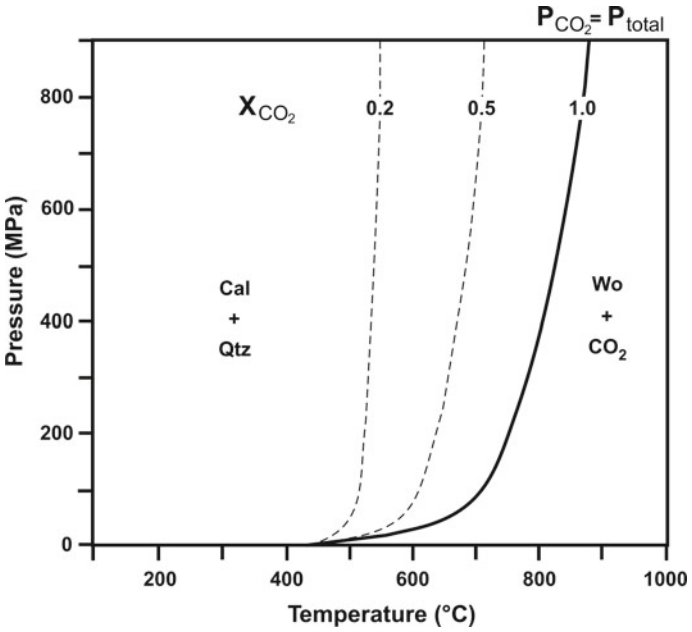

Fig. 3.17 Univariant decarbonation curves for the reaction Cal + Qtz = Wo + CO_2 as a function of *T–P* ($P_{fluid} = P_{CO_2}$) and fluid composition (X_{CO2})

However, the fluid composition in most carbonate-bearing rocks can be assumed to be a binary mixture of CO_2 and H_2O. One compositional variable is therefore sufficient to describe the fluid composition. Usually this variable is defined as the mole fraction of CO_2 in the fluid (X_{CO_2}). X_{CO_2} is zero in pure H_2O fluids and equal to one in pure CO_2 fluids. Consider the following characteristic mixed volatile reaction:

$$\text{margarite} + 2\ \text{quartz} + \text{calcite} = 2\ \text{anorthite} + 1\ CO_2 + 1\ H_2O \qquad (3.18)$$

For pure solid phases, the equilibrium constant is, $K_{P,T} = a_{CO_2}\, a_{H_2O}$. Equilibrium conditions depend on the activities of CO_2 and H_2O in addition to pressure and temperature. However, if we assume that the fluid is a binary CO_2-H_2O mixture (and using an ideal solution model for the fluid; a = X), the equilibrium constant reduces to, $K_{P,T} = X_{CO_2}(1 - X_{CO_2})$ or $K_{P,T} = X_{CO_2} - (X_{CO_2})^2$. Depending on the actual value of the equilibrium constant at *P* and *T*, this quadratic equation may have no, one or two solutions. The equilibrium conditions of the margarite breakdown reaction (3.18) is visualized as a complex surface in *P–T*- X_{CO_2} space. Because it is inconvenient to work graphically in a three-dimensional space, mixed volatile reactions are most often represented on isobaric *T-X* diagrams or isothermal *P-X* diagrams, depending on the geological problem one wants to solve. It is also possible to select a certain metamorphic *P–T* field gradient that best describes the

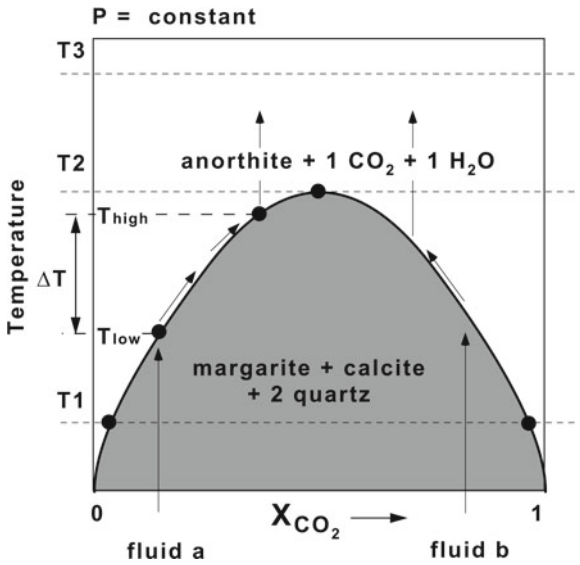

Fig. 3.18 Schematic equilibrium conditions of a mixed volatile reaction (isobaric *T–X* diagram)

regional metamorphic area under consideration and construct (*P–T*)-X_{CO_2} sections (examples are given in Chap. 6). For instance, take the case where P is kept constant. The quadratic equation above can be solved for a series of temperatures and the results shown on an isobaric *T-X* section (Fig. 3.18). At T_1 the four-mineral assemblage, margarite + quartz + calcite + anorthite, may coexist with either very H_2O-rich or very CO_2-rich fluids. At one unique temperature, T_2, the equation has only one solution. Temperature T_2 represents the maximum temperature for the reactant assemblage, as above it, no margarite, calcite and quartz can coexist. At T_3 no (real) solution for the equation exists and the product assemblage may coexist with binary CO_2-H_2O fluids of any composition. The heavy solid curve in Fig. 3.18 connects all solutions of the equilibrium constant equation and represents the reaction equilibrium of the margarite breakdown reaction in quartz- and calcite-bearing rocks. The curve separates a *T-X* field where the reactants are stable (shaded) from an area where the products are stable. At any temperature < T_2, the products are stable in H_2O-rich or CO_2-rich fluids, respectively. The reactants may coexist with fluids of intermediate composition.

Consider now a margarite-bearing rock containing excess quartz and calcite and a pore fluid of composition "***a***". Adding heat to this rock raises its temperature until the reaction boundary is reached at T_{low}. Further temperature increase causes the production of anorthite and a fluid with equal proportions of CO_2 and H_2O (Eq. (3.18)). Because the produced fluid is more CO_2-rich than the original pore fluid of the rock (fluid ***a***), the total fluid composition is driven to more CO_2-rich compositions. The original fluid becomes progressively more diluted with the fluid produced by the reaction; ultimately the fluid is entirely dominated by the reaction fluid and has the composition $X_{CO_2} = 0.5$ (1 mol CO_2 and 1 mol H_2O). This will

be the case at T_2, the maximum temperature of the reactant assemblage. However, the reactant assemblage may become exhausted with respect to one or more reactant minerals before reaching T_2. For example, if the original rock contains 1 mol margarite, 3 mol calcite and 5 mol quartz per 1000 cm^3, the reaction will consume all margarite during the reaction progress at some temperature along the isobaric univariant curve (T_{high}). The rock consists then of anorthite, calcite and quartz, and a fluid of the composition at T_{high}. Further addition of heat will increase the temperature of the rock, but the fluid composition will remain unchanged. Therefore, the univariant assemblage margarite + anorthite + calcite + quartz is stable over a temperature interval ΔT and coexists with fluids with increasing CO_2 content. The temperature interval ΔT is also associated with gradual changes in modal composition in the rock. At T_{low} the first infinitesimally small amount of anorthite appears and it continuously increases in modal abundance as the reaction progresses towards T_{high} where the last small amount of margarite disappears. The fluid composition at the maximum temperature T_2 depends exclusively on the reaction stoichiometry. Consider the reaction that makes olivin marbles from tremolite marbles:

$$11 \text{ dolomite} + \text{tremolite} = 13 \text{ calcite} + 8 \text{ forsterite} + 9 \text{ } CO_2 + 1 \text{ } H_2O \qquad (3.19)$$

In this reaction, the produced fluid has the composition $X_{CO_2} = 0.9$ (9 mol CO_2 and 1 mol H_2O) and the temperature maximum of the equilibrium is at the same fluid composition. The general shape of reaction equilibria for reactions of the type: $a = b + m\ H_2O + n\ CO_2$ (both fluid species are products of the reaction) is shown in Fig. 3.19 together with mixed volatile reactions with other reaction stoichiometries.

The equilibrium constant of the reaction:

$$2 \text{ zoisite} + 1 \text{ } CO_2 = 3 \text{ anorthite} + \text{calcite} + 1 \text{ } H_2O \qquad (3.20)$$

can be written as, $K = (1/X_{CO_2}) - 1$. It varies between zero and + ∞ (ln K -∞, + ∞). Consequently, the univariant assemblage coexists with CO_2-rich fluids at low temperatures and with H_2O-rich fluids at high temperatures. The general shape of reactions a + CO_2 = b + H_2O can be seen in Fig. 3.19. The reaction that produces tremolite marbles from siliceous dolomitic limestone:

$$8 \text{ quartz} + 5 \text{ dolomite} + 1 \text{ } H_2O = \text{tremolite} + 3 \text{ calcite} + 7 \text{ } CO_2 \qquad (3.21)$$

represents a reaction of the type: a + H_2O = b + CO_2 and has, compared to reaction (3.20), an inverse shape in *T-X*-diagrams (Fig. 3.19). It follows from the earlier discussion on pure dehydration and decarbonation reactions (see Figs. 3.16, 3.17) that they must have general curve shapes as shown in Fig. 3.19. The figures presented so far also permit a deduction of the general shape of mixed volatile reaction equilibria in isothermal *P-X* sections (you may try to draw a *P-X* figure at constant temperature similar to Fig. 3.19).

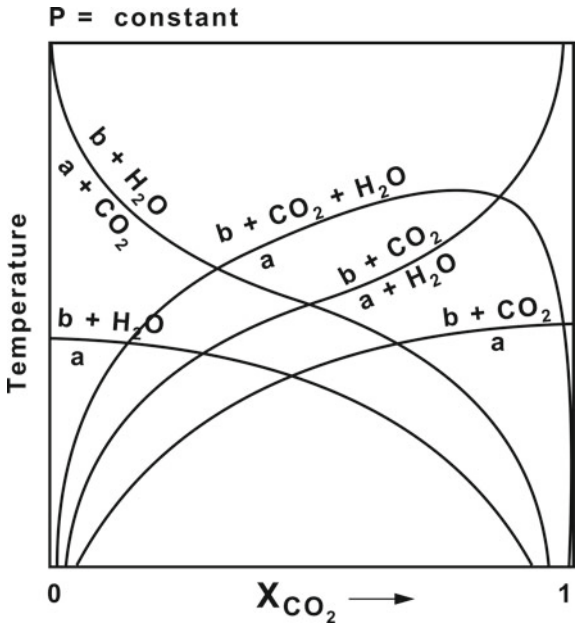

Fig. 3.19 Schematic equilibrium conditions of mixed volatile reactions with different reaction stoichiometry (isobaric *T*–*X* diagram)

3.6.2.4 Oxidation/Reduction Reactions

A number of cations making up minerals occur in different oxidation states. Examples are, Fe^{2+}/Fe^{3+}, Cu^{+}/Cu^{2+}, Mn^{2+}/Mn^{3+}. The most important REDOX couple in common rock-forming silicates and oxides is Fe^{2+}/Fe^{3+}. The two iron oxides hematite and magnetite are related by the reaction:

$$6\ Fe_2O_3 = 4\ Fe_3O_4 + O_2 \tag{3.22}$$

The equilibrium conditions of this reaction are given (for pure hematite and magnetite) by, $K = a_{O_2}$. Again, the equilibrium depends on three variables; *P*, *T* and a_{O_2}. As the pressure dependence is very small for this REDOX reaction, the equilibrium is commonly depicted on isobaric *T* versus $\log a_{O_2}$ diagrams (Fig. 3.20). In the literature, the activity is often replaced by f_{O_2} (fugacity of O_2). $\ln f_{O_2}$ is numerically identical to $\log a_{O_2}$ if an appropriate standard state is chosen. The fugacity is close to the partial pressure of O_2 under low pressure conditions. However, fugacity can be related to the partial pressure of O_2 at any pressure. The partial pressure of O_2 in crustal metamorphic rocks is extremely small (on the order of 10^{-20}–10^{-40} bar). However, coexistence of hematite and magnetite may also be formulated in the presence of water as,

$$6\ Fe_2O_3 + 2\ H_2 = 4\ Fe_3O_4 + 2\ H_2O \tag{3.23}$$

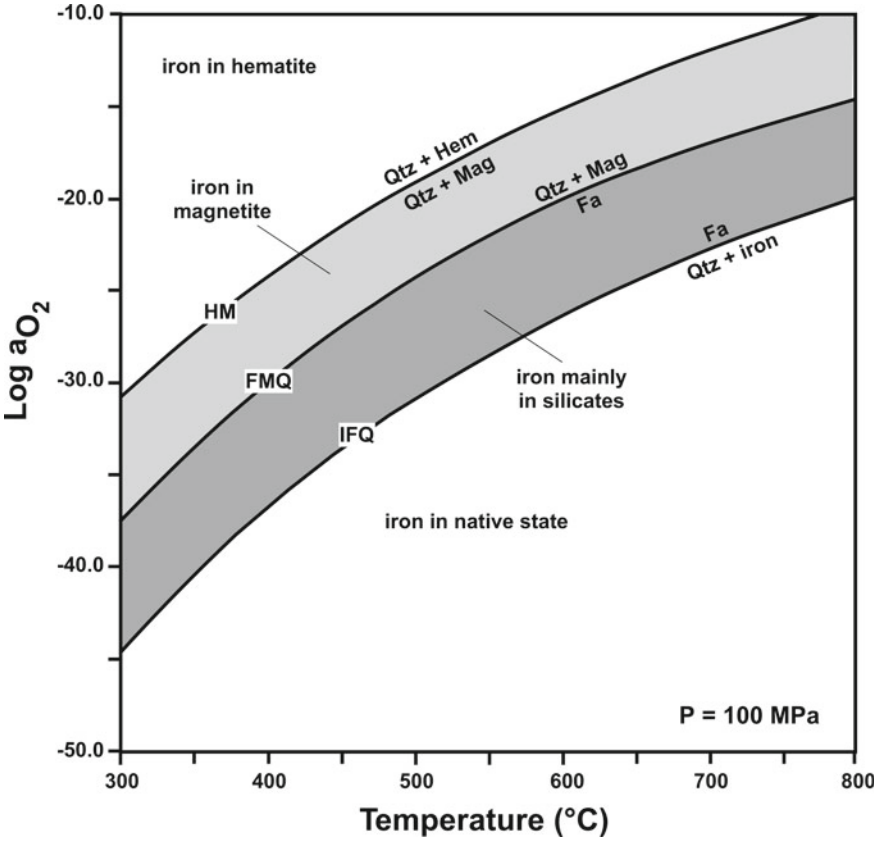

Fig. 3.20 Log oxygen activity—*T* diagram showing various oxidation states of iron in the system Fe–Si–O at 100 MPa. Oxygen is fixed along curves by the mineral assemblages HM = hematite-magnetite; FMQ = fayalite-magnetite-quartz; IFQ = iron-fayalite-quartz. Standard state for O_2: pure gas at T and 10^5 Pa

and the equilibrium can be shown on *T* versus $\log a_{H_2}$ diagrams. The assemblage biotite + K-feldspar + magnetite is common in high-grade metamorphic and in igneous rocks. The REDOX reaction:

$$\underset{\text{biotite(annite)}}{2\,KFe_3AlSi_3O_{10}(OH)_2} + O_2 = \underset{\text{K-feldspar}}{2KAlSi_3O_8} + \underset{\text{magnetite}}{2Fe_3O_4} + 2H_2O \qquad (3.24)$$

depends on O_2 (and H_2O). If O_2 is increased then biotite is oxidized to Kfs + Mag, if O_2 is lowered then Kfs + Mag is reduced to biotite (Fig. 3.21). Expressed in another way, the three mineral assemblage, Bt + Kfs + Mt, defines the activity of O_2 in the presence of water.

The model reaction (3.24) helps to understand the REDOX behaviour of Fe^{2+}-bearing silicate minerals such as micas, amphiboles and pyroxenes in general. The

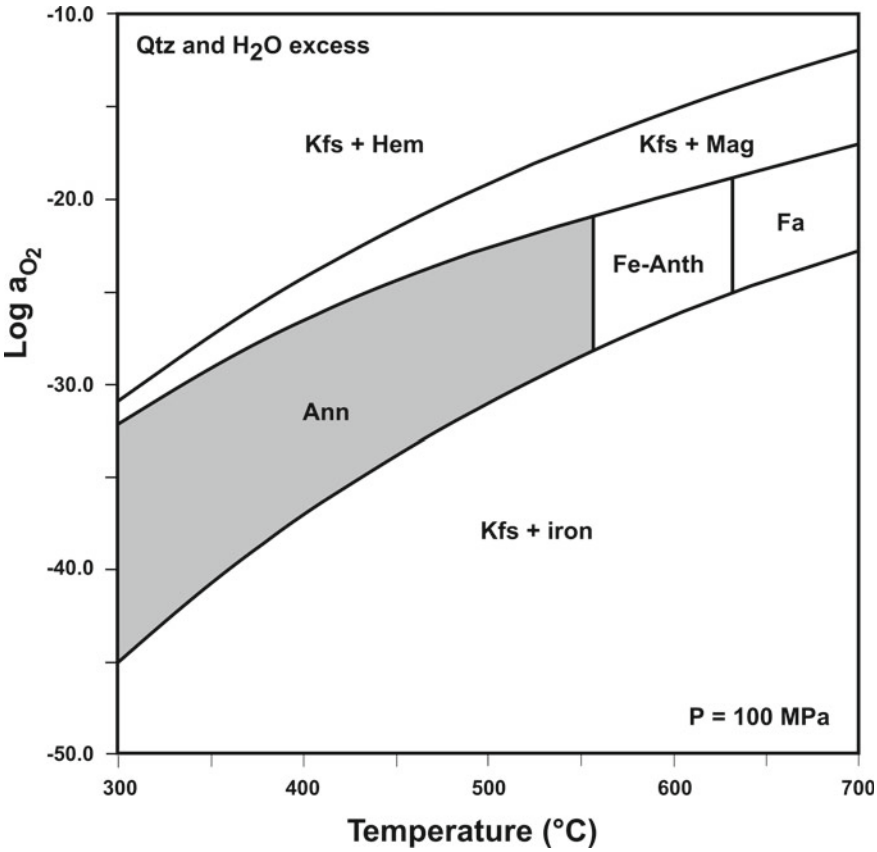

Fig. 3.21 Log oxygen activity—*T* diagram at 200 MPa showing stability fields for Fe-biotite (annite) (shaded field), Fe-anthophyllite, fayalite, and K-feldspar (microcline/sanidine) coexisting with iron, magnetite, hematite, in the presence of excess quartz and water. Standard state for O_2: pure gas at T and 10^5 Pa

reaction transfers the Fe-biotite component annite to feldspar and Fe-oxide thus leaving behind the Mg-biotite component phlogopite in the mica. Hence, the Mg/Fe ratio of silicates, the ferrous/ferric ratio of coexisting oxides, and oxygen activity are interrelated. At high a_{O_2} Fe–Mg silicates tend to be Mg-rich and coexist with hematite and at lower a_{O_2} silicates contain less of the Mg phase component and tend to occur with magnetite ± ilmenite under at the same temperature. In layered rocks with contrasting silicate + oxide assemblages, this implies that the rocks have retained the oxidation state of their protolith and that oxygen activity is controlled by the mineral assemblage of the rocks. Where extensive reaction with a fluid phase during metamorphism has occurred such primary oxidation variation may be eliminated and the oxygen activity is imposed externally.

REDOX reactions do not necessarily involve molecular gass species. Redox reactions may also be formulated in ionic form (e.g. the Mag–Hem reaction):

$$2\ Fe_3O_4 + H_2O = 3\ Fe_2O_3 + 2\ H^+ + 2\ e^- \tag{3.25}$$

Oxidation of magnetite to hematite in the presence of water produces two H^+ and two electrons. This formulation shows that oxydation produces electrons, reduction consumes electrons ($Fe^{2+} = Fe^{3+} + e^-$). The magnetite–hematite reaction (3.25) depends on the REDOX potential ($p_e = -\log a_e-$) and on the activity of the hydrogen ion ($p_H = -\log a_{H^+}$). . Graphical representation of equilibria of the type (3.25) is often done by means of p_e (oxidation potential) versus p_H diagrams (see many examples in the classic textbook Garrels and Christ 1965).

3.6.2.5 Reactions Involving Sulfur

Sulfides are widespread accessory minerals in metamorphic rocks. Most common are pyrrhotite (FeS) and pyrite (FeS_2). If both Fe-sulfides occur in a metamorphic rock, their stable coexistence requires equilibrium of the reaction:

$$2\ FeS_2 = 2\ FeS + S_2 \tag{3.26}$$

The dominant sulfur species in metamorphic fluids is either H_2S or SO_2. If one wishes to discuss sulfide-involving reactions in terms of the most abundant species, Eq. (3.26) can be rewritten in the presence of water ($2H_2O = 2H_2 + O_2$; $2H_2S = 2H_2 + S_2$) as:

$$FeS_2 + H_2 = FeS + H_2S \tag{3.27}$$

Graphical representation of sulfide-involving reactions depends on the actual problem but partial pressure (activity, fugacity) of a sulfur species in the fluid versus temperature diagrams are popular. If sulfide reactions are combined with REDOX reactions, oxygen (hydrogen) versus sulfur diagrams are useful. As an example, Fig. 3.22 shows the phase relationships among some iron oxides and sulfides in terms of a_{H_2} and a_{H_2S}. . The diagram shows that the presence of one Fe-sulfide and one Fe-oxide in a metamorphic rock (e.g. magnetite and pyrrhotite) fixes the activities of H_2 and H_2S to distinct values along a univariant line at a given *P* and *T* in the presence of water. Rocks may be zoned with respect to oxides and sulfides depending on gradients in a_{H_2S}, e.g. under reducing conditions, rocks may contain magnetite, pyrrhotite or pyrite with increasing a_{H_2S}.

3.6.2.6 Reactions Involving Halogens

Fluorine and chlorine may replace OH groups in all common rock-forming hydrous minerals, notably mica, talc and amphibole (less so in serpentine minerals and chlorite). The halogen content of common rock-forming minerals may be related to

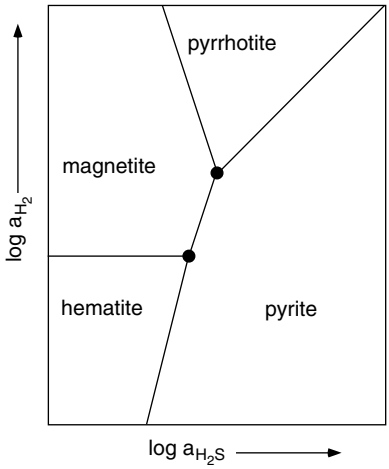

Fig. 3.22 Qualitative phase relationships among hematite, magnetite, pyrrhotite and pyrite in a log a_{H2} versus log a_{H2S} activity-activity diagram

exchange reactions of the type (e.g. fluorine-hydroxyl exchange between biotite [phlogopite] and fluid):

$$KMg_3AlSi_3O_{10}(OH)_2 + 2\ HF = KMg_3AlSi_3O_{10}(F)_2 + 2\ H_2O \qquad (3.28)$$

Also in this case, equilibria of the type (3.28) are commonly shown and discussed in terms of partial pressure (fugacity, activity) of a gaseous halogen species (HCl, HF) versus temperature diagrams or in terms of μ-μ-diagrams (or activity-activity diagrams).

3.6.2.7 Complex Mixed Volatile Reactions and Fluids

It is a common situation in metamorphic rocks that they contain simultaneously halogen-bearing hydrous silicates, carbonates, sulfides, and oxides. Dealing with such rocks consequently means that all types of metamorphic reactions must be considered together. For example, consider a typical calcareous mica schist containing the minerals: calcite, quartz, K-feldspar, plagioclase, muscovite, biotite, graphite and pyrite. Among the minerals and nine potentially important fluid species the following linearly independent equilibria can be written:

(a) Equilibria involving silicates, sulfides and carbonates

$$KAl_2AlSi_3O_{10}(OH)_2 + CaCO_3 + 2\ SiO_2 = KAlSi_3O_8 + CaAl_2Si_2O_8 + H_2O + CO_2$$

$$KFe_3AlSi_3O_{10}(OH)_2 + 3\ S_2 = 2\ KAlSi_3O_8 + 3\ FeS_2 + H_2O$$

(b) Equilibria involving graphite

$$C + O_2 = CO_2$$
$$C + 2\,H_2 = CH_4$$
$$2\,C + O_2 = 2\,CO$$

(c) Equilibria involving fluid species only

$$2\,H_2O = 2\,H_2 + O_2$$
$$S_2 + 2\,H_2 = 2\,H_2S$$
$$S_2 + 2\,O_2 = 2\,SO_2$$

A mass action equation can be formulated for all eight equilibria [see, for example Eq. (3.16)]. Mass action equations express the equilibrium constant in terms of activities at constant pressure and temperature. In addition, in the presence of a free fluid phase in the rock, the following mass balance equation (total pressure equation) can be written:

$$p_{total} = p_{fluid} = p_{H_2O} + p_{CO_2} + p_{O_2} + p_{H_2} + p_{CH_4} + p_{CO} + p_{S_2} + p_{H_2S} + p_{SO_2}$$

Equation (d9) states that the sum of the partial pressures of the fluid species is equal to the total lithostatic rock pressure. Together with activity (fugacity)—partial pressure functions for the species in the fluid, the set of nine equations can be solved iteratively for the nine unknown partial pressures and hence the fluid composition. This means that the mineral assemblage of the calcareous mica schist defines and completely controls the composition of the coexisting fluid phase at any given pressure and temperature. In other words, the minerals of the rock **buffer** the fluid composition. In most metamorphic fluids the partial pressures of O_2 and CO are extremely low compared with the total pressure. H_2 is usually also low in most metamorphic fluids. The dominant sulfur species in the fluid is H_2S at low temperatures and SO_2 at high temperatures. CH_4 may be high in some fluids at lower temperature. CO_2 is dominant at higher temperatures.

3.6.2.8 Reactions Involving Minerals and Dissolved Components in Aqueous Solutions

The fluids that are associated with rock metamorphism in crust and mantle inevitably migrate from the source area. They come in contact with other rocks with which they may not be in equilibrium. Chemical reactions that attempt to establish equilibrium between the solid rock assemblage and the fluid are termed "**fluid-rock interactions**". Fluid-rock interaction is important in, for example, the formation of hydrothermal ore deposits, contact metasomatism, large-scale infiltration and reaction during orogenesis, in shear zone metasomatism, fissure mineral deposition and in geothermal fields. As an example, take a crustal volume containing rocks with the assemblage margarite + calcite + quartz (Fig. 3.18). An externally-derived fluid with the composition $X_{CO_2} = 0.01$ infiltrates this rock at T_{high}. The fluid is in

equilibrium with the product assemblage of reaction (3.18) rather than with the reactant assemblage that is actually present. A consequence of fluid infiltration is that the fluid will drive the reaction until all margarite disappeared and the rock contains the anorthite + calcite + quartz assemblage. In this case the rock cannot buffer the fluid composition and its assemblage is controlled by the external fluid.

Commonly, metamorphic fluids are saline brines containing high concentrations of metal ions and complexes. Therefore, infiltrating fluids may also have a cation composition that is not in equilibrium with the solid phase assemblage it comes in contact with. An essential aspect of fluid-rock interaction is the reaction of phase components of the solid mineral assemblage of the rock and dissolved species in the external fluid. Some examples:

1. Formation of talc schist by interaction of serpentinite with silica-rich fluids:

$$Mg_3Si_2O_5(OH)_4 + 2\ SiO_{2_{aq}} = Mg_3Si_4O_{10}(OH)_2 + H_2O \tag{3.29}$$

   where $SiO_{2,aq}$ refers to an uncharged hydrous silica complex in the aqueous fluid. In many cases, the SiO_2-rich fluid infiltrating the serpentinite is saturated with respect to quartz, which results from interaction of the fluid with granitic gneiss or quartzo-feldspathic schist that encloses the serpentinite body.
2. Formation of soapstone (Tlc + Mgs rock) by interaction of serpentinite with CO_2-bearing fluids:

$$2\ Mg_3Si_2O_5(OH)_4 + 3\ CO_2 = Mg_3Si_4O_{10}(OH)_2 + 3\ MgCO_3 + 3\ H_2O \tag{3.30}$$

3. Sericitization of K-feldspar is a widespread process during retrograde metamorphism:

$$\underset{K-feldspar}{3\ KAlSi_3O_8} + 2\ H^+ = \underset{muscovite(sericite)}{KAl_3Si_3O_{10}(OH)_2} + 2\ K^+ + 6\ SiO_{2_{aq}} \tag{3.31}$$

The type of reaction (3.31) is important in geology and is referred to as a **hydrolysis reaction**. Any other kind of metamorphic mineral reaction can be viewed as a linear combination of a series of hydrolysis reactions. For example, the phase transition kyanite = sillimanite can be considered as a result of two simultaneously progressing hydrolysis reactions (Carmichael 1968):

$$\text{Ky hydrolysis (dissolution):}\quad Al_2SiO_{5_{Ky}} + 6\ H^+ = 2\ Al^{3+} + SiO_{2_{aq}} + 3\ H_2O \tag{3.32}$$

$$\text{Sil precipitation :}\quad 2\ Al^{3+} + SiO_{2_{aq}} + 3\ H_2O = Al_2SiO_{5_{Sil}} + 6\ H^+ \tag{3.33}$$

$$\text{net-reaction } (3.32 + 3.33) :\quad Al_2SiO_{5_{Ky}} = Al_2SiO_{5_{Sil}} \tag{3.34}$$

In extremely acid aqueous fluids, Al^{3+} is the dominant Al species, but similar reactions can be written with other Al species such as $Al(OH)^{2+}$, $Al(OH)_2^+$, $Al(OH)_3^\circ$, $Al(OH)_4^-$, depending on the pH of the fluid.

The above example of the Ky = Sil reaction illustrates the most efficient mechanism by which old unstable minerals or mineral assemblages are replaced by more stable ones. The unstable reactant minerals dissolve in the aqueous solution because they have a higher solubility than the stable product minerals. The more stable minerals and mineral assemblages precipitate from the aqueous solution after a certain threshold degree of supersaturation is reached and nucleation and growth of the reaction products begin. This general process mechanism of dissolution and precipitation involves an aqueous fluid and is fundamental to water–rock interaction in hydrothermal and geothermal systems (and weathering, diagenesis and other near surface processes as well). However, it is also expected to be the most efficient processes mechanism in metamorphism at high *P–T* conditions. Strong evidence for this claim is, that in high-grade metamorphism structural disequilibrium and persistence of metastable assemblages increases with grade. This is unexpected at a first glimpse because reaction kinetics and diffusive transport is favored by increasing temperature. However, at high P and T metamorphic rocks tend to lose the aqueous fluid and thus the efficient dissolution–precipitation mechanism vanishes with the fluid.

The expression dissolution–precipitation mechanism does not necessarily mean dissolution first followed by precipitation. The growth of a new mineral may exert pressure on the neighboring grains thereby increasing their solubility by the mechanism of pressure-solution well known from sedimentary rocks. The overall process precipitates first then it dissolves (Merino and Canals 2011).

A further important fluid-rock interaction process is the albitization of K-feldspar. It is an **ion exchange reaction** that occurs during low-grade alteration of granite and granite-gneiss:

$$KAlSi_3O_{8_{K-feldspar}} + Na^+ = NaAlSi_3O_{8_{Na-feldspar}} + K^+ \qquad (3.35)$$

Ionic (complex) reactions can be represented by means of p_H versus gas pressure (activity, fugacity) diagrams, activity-activity diagrams (or μ-μ diagrams), activity-temperature diagrams, etc., depending on the actual geological problem. A computed quantitative activity-activity diagram for the system Na–K–Al–Si–O–H (Fig. 3.23) shows the fields for alkali-feldspars (K-feldspar and albite), micas (muscovite, paragonite), and an Al–silicate with respect to the activity of alkali oxides. The diagram shows that at low a_{K_2O} and a_{Na_2O}, Al–silicate is stable, whereas the opposite stabilizes feldspars. Micas are present at intermediate activities of alkali oxides. The activities of the alkali metal oxides can be converted to conventional ionic species in an aqueous fluid by the equations: $Na_2O + 2H^+ = 2\ Na^+ + H_2O$ and $K_2O + 2H^+ = 2\ K^+ + H_2O$ corresponding to $\log a_{Na_2O} =$

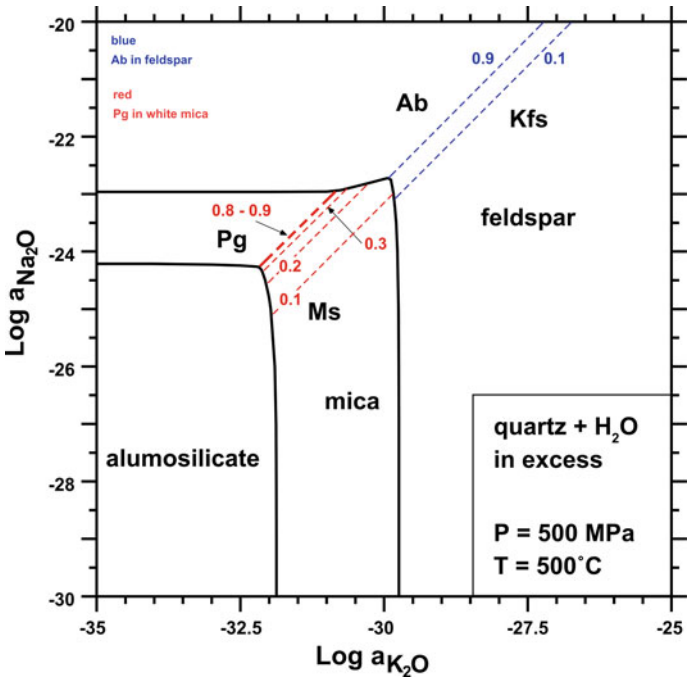

Fig. 3.23 Computed, quantitative activity-activity diagram for the system Na–K-Al-Si–O-H showing the fields for feldspar, mica and alumosilicate at fixed *P*–*T* conditions

$2\log(a_{Na^+}/a_{H^+})$ and $\log a_{K_2O} = 2\log(a_{K^+}/a_{H^+})$. The phase boundaries are markedly curved near the transitions of Kfs to Ab and Ms to Pg as a result of Na K^{-1} exchange in Fsp and white mica.

3.7 Reaction Progress

Chemical reactions in rocks proceed in response to gradients in intensive variables (e.g. increase in temperature). The progress of a chemical reaction can be illustrated by using the wollastonite-producing reaction (Fig. 3.17) as an example:

$$CaCO_3 + SiO_2 = CaSiO_3 + CO_2 \tag{3.36}$$

Calcite and quartz may react and produce wollastonite and release CO_2 gas. The equilibrium conditions of the reaction are shown in Fig. 3.24 as a function of temperature and the composition of a binary CO_2–H_2O fluid at a total pressure of 200 MPa. A calcite- and quartz-bearing rock with an initial pore space of 1% may contain a fluid of the composition $X_{CO_2} = 0.01$. Adding heat to this rock brings it to the reaction boundary of the wollastonite-producing reaction at a temperature of

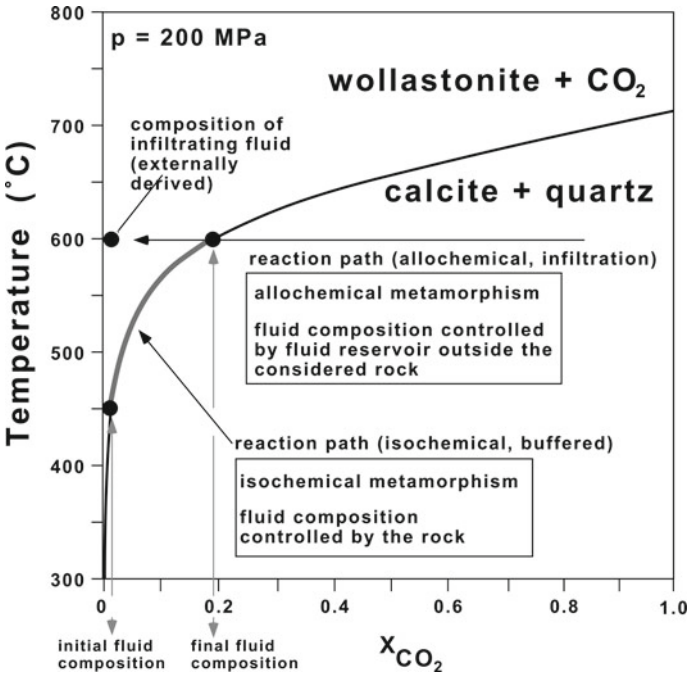

Fig. 3.24 Quantitative temperature versus fluid composition phase diagram showing the equilibrium conditions of the wollastonite reaction at 200 MPa

about 450 °C. Further addition of heat will produce wollastonite and the fluid becomes enriched in CO_2 as a result of CO_2 released by the reaction. Suppose the rock finally reaches a temperature of 600 °C and contains the isobaric univariant assemblage calcite + quartz + wollastonite. It is a simple matter to calculate the modal amount of wollastonite produced by the reaction:

Reference volume: 1000 cm^3 rock
1% pore space = 10 cm^3 fluid per 1000 cm^3
Cal + Qtz reaches equilibrium with Wo at 450 °C (200 MPa) and $X_{CO_2} = 0.01$ (Fig. 3.24)
Cal + Qtz + Wo assemblage at 600 °C (200 MPa) and $X_{CO_2} = 0.19$ (Fig. 3.24)
Molar volume of H_2O at 450 °C, 200 MPa = 24 cm^3 $mole^{-1}$ (Fig. 3.11)
Initial fluid 99 mol % H_2O + 1 mol % CO_2 (assume for simplicity pure H_2O)
Number of moles of H_2O in the initial fluid: $n^{\circ}_{H_2O} = 10/24 = 0.42$ moles H_2O
Initial $X^{\circ}_{CO_2} = n^{\circ}_{CO_2} / \left(n^{\circ}_{CO_2} + 0.42 \right)$

Final $X^{f}_{CO_2} = n^{f}_{CO_2} / \left(n^{f}_{CO_2} + 0.42 \right)$
Solving for:
Number of moles of CO_2 in the initial fluid: $n^{\circ}_{CO_2} = 4.21$ mmoles
Number of moles of CO_2 in the final fluid: $n^{f}_{CO_2} = 96.6$ mmoles
CO_2 produced by the reaction: $\Delta n_{CO_2} = n^{f}_{CO_2} - n^{\circ}_{CO_2} = 96.55 - 4.21 = 92.34$ mmoles
With reference to Eq. (3.35): 92.34 mmoles CO_2 is equivalent to 92.34 mmoles of wollastonite produced by the reaction per 1000 cm^3 rock
The molar volume of wollastonite is: V° = 40 cm^3 $mole^{-1}$
Wollastonite produced by buffered reaction: 3.7 cm^3 (0.367 vol.%)

The amount of wollastonite is very small and would hardly be detected under the petrographic microscope.

Let us now consider a calcite- and quartz-bearing rock with 20 vol. % wollastonite that equilibrated at 600 °C and 200 MPa. From the calculations above it is evident that isochemical metamorphism can produce only a very small modal amount of wollastonite (at 600 °C and 200 MPa). Consequently, a very wollastonite-rich rock that formed at these conditions must be the result of interaction of the rock with an externally-derived H_2O-rich fluid that pushed conditions across the reaction equilibrium into the wollastonite field shown in Fig. 3.24. The question is how much H_2O must be added to the rock in order to produce the observed modal proportion of wollastonite? This can be readily calculated:

20 vol.% wollastonite (V° = 40 cm^3 $mole^{-1}$) = 0.5 mole/100 cm^3
The rock contains 5 mol wollastonite/1000 cm^3 rock. It follows from the reaction stoichiometry of reaction (3.35) that the reaction also produced 5 mol of CO_2
However the final $X^{f}_{CO_2} = n^{f}_{CO_2} / \left(n^{f}_{CO_2} + n_{H_2O} \right)$ is equal to 0.19 (Fig. 3.24)
Solving for: $n_{H_2O} = n^{f}_{CO_2} \left(1 - X^{f}_{CO_2} \right) \left(1 / X^{f}_{CO_2} \right)$
gives: $n_{H_2O} = 5 \times 0.81 \times (1/0.19) = 21.315$ moles H_2O
The molar volume of H_2O is: V° (600 °C, 200 MPa) = 31 cm^3 (Fig. 3.11)
The total volume of H_2O that reacted with the rock is: $V_{H_2O} = 660\ cm^3/1000\ cm^3$ rock

In conclusion, a rock with 20 vol.% wollastonite that formed from calcite + quartz at 600 °C and 200 MPa requires interaction with 660 cm^3 H_2O per 1000 cm^3 rock. This represents a minimum value. If the composition of the interacting fluid is more CO_2-rich, more fluid is required to produce the observed amount wollastonite in the rock. The deduced amount of interacting external fluid may be expressed in terms of a time-integrated **fluid to rock ratio**: fluid-rock ratio = 660 cm^3/1000 cm^3 = 0.66.

3.8 Phase Diagrams

3.8.1 Phase Diagrams, General Comments and Software

Phase diagrams display equilibrium relationships among phases and phase assemblages in terms of intensive, extensive or mixed variables. A widely used type of phase diagram in metamorphic petrology is the *P–T* diagram. It shows the equilibrium relationships among minerals (and fluids) as a function of the intensive variables pressure and temperature. The chosen ranges of the parameter values define a *P–T* window that is appropriate for the problem of interest. Mineral and fluid compositions may be constant or variable on such a diagram. Composition phase diagrams show the phase relationships in terms of extensive variables at specified values of pressure and temperature. AFM and ACF diagrams described in Chap. 2 are examples of such composition phase diagrams.

Phase diagram software is routinely used to compute and display petrologic phase diagrams from published sets of thermodynamic data of phase components and models of the thermodynamic properties of fluid and solid solutions. All phase diagrams in this book were computed by using the program package THERIAK/DOMINO, a multipurpose software system that permits the construction of remarkably complex phase diagrams (de Capitani and Petrakakis 2010) together with updated versions of the data base of Berman (1988). A helpful introduction to the Theriak/Domino application package can be found on a webpage maintained by Dexter Perkins (https://serc.carleton.edu/research_education/equilibria/theriak-domino.html). Some diagrams are based on SUPCRTBL (Zimmer et al. 2016). For further information visit the highly recommended webpage of Chen Zhu at Bloomington (https://models.earth.indiana.edu/applications_index.php).

Other petrologic computer codes include (see Chap. 4 for more information about some of these programs): GEØCALC by Berman et al. (1987); PERPLE_X by Connolly and Kerrick (1987); Connolly (1990); Connolly (2009), THERMOCALC by Powell and Holland (1985, 1988); TWQ or TWEEQU by Berman (1991); SUPCRT92 by Johnson et al. (1992); PTPATH by Spear et al. (1991) and THERMO by Perkins et al. (1987). Compilations of thermodynamic data for substances of geologic interest are found in Clark (1966); Burnham et al. (1969); Stull and Prophet (1971); Robie et al. (1978); Helgeson et al. (1978); Holland and Powell (1985); Powell and Holland (1985); Powell and Holland (1988); Berman (1988); Holland and Powell (1990,

1998, 2011); Johnson et al. (1992); Zimmer et al. (2016). Recent thermodynamic mixing models for solid solution minerals and melts include: Diener and Powell (2012) for amphiboles and pyroxenes; Green et al. (2016) for melts in metabasites, Holland et al. (2018) for partial melts in ultramafic to granitic rocks; White et al. (2014) for minerals in metapelitic rocks.

The thermodynamic data sets of Berman (1988) and Holland and Powell (1990, 1998, 2011) are classified as so-called internally consistent data sets because of the specific data retrieval technique used in deriving the data. These two sets are particularly well suited for use in conjunction with the two mentioned programs and are widely used by metamorphic petrologists. Thermodynamic data can be derived from calorimetric measurements and, especially, from experimental phase equilibrium data. Nearly all phase diagrams shown in this book have been generated by THERIAK/DOMINO using the RB88 data base (or updated versions of it).

Phase diagrams are indispensable tools for the description, analysis and interpretation of metamorphic rocks and metamorphism. The ability to read and understand phase diagrams is central and essential in metamorphic petrology. The capability to calculate and construct phase diagrams is important for all those who are in need of phase diagrams for phase assemblages and phase compositions that are unique for the geologic problem in question. It may also be necessary to modify published phase diagrams and adapt them to the actual problem, e.g. change the P–T frame or other parameter values or modify solid solution models or add data for new phase components to the data base.

It is also clear, that phase diagrams depict the equilibrium state of a system and thus represent the target configuration for a system adjusting to disequilibrium. They give the framework for the ultimate order when processes and reactions cease and come to an end. However, it is a terribly trivial insight that metamorphism is more than phase diagrams. Metamorphic processes and reactions are caused by disequilibrium in the system as discussed in various parts of the text so far. Reaction kinetics and local mass transfer coupled with deformation determine the structure of metamorphic rocks and control how close the mineral assemblages approach the equilibrium case depicted on phase diagrams.

3.8.2 The Phase Rule

Although it is not the intention of this book to give a comprehensive treatment of the computation and construction of phase diagrams, it is useful to briefly introduce two important aspects of phase diagrams: the phase rule and Schreinemakers rules.

The state of a heterogeneous system, such as a rock, depends on a number of state variables such as pressure, temperature and chemical potentials. The requirements of heterogeneous equilibrium impose some restrictions on these variables (equilibrium constraints). The phase rule relates the number of variables in a system and the number of equations that can be written among them at equilibrium. In a system with a total number of c components and composed of p phases the number of variables is:

- for each phase: *T, P*, and c−1 compositional variables = c + 1
- for the system of *p* phases: p(c + 1).

Equilibrium constraints:
The temperature of all phases must be the same (thermal equilibrium) ⇒

- p − 1 equations of the type: T of phase α = T of phase β.

The pressure on all phases must be the same (mechanical equilibrium) ⇒

- p − 1 equations of the type P on phase α = P on phase β.

The chemical potential of component *i* must be the same in all phases (chemical equilibrium) ⇒

- c(p − 1) equations of the type $\mu_{i\alpha} = \mu_{i\beta}$; p−1 equations for each component from 1 to c.

Hence, the number of variables n_v is: p(c + 1), and the number of equations n_e: 2 (p − 1) + c(p− 1).

Now let us define a variable f as the difference between n_v and n_e. f simply expresses how many variables can be changed independently in a system at equilibrium.

$f = n_v - n_e = [p(c+1) - 2(p-1) - c(p-1)]$; or simply

$$\mathbf{f = c + 2 - p} \tag{3.37}$$

This equation is known as the **phase rule**. f is often referred to as **variance** or **degrees of freedom** of the system. A consequence of the phase rule is that the number of phases cannot exceed the number of components by more than 2.

In a one-component system (e.g. Al_2SiO_5) consisting of one phase (e.g. kyanite), there are two variables which can be varied independently, i.e. *P* and *T*. If there are two phases present (sillimanite and kyanite), only one variable can be specified independently. If there are three phases present (andalusite, sillimanite and kyanite), the number of variables equals the number of equations (f = 0) and the system of equations has one unique solution. In other words, coexistence of all three aluminosilicates completely defines the state of the system and this is only possible at a unique value of *P* and *T* (the triple point, invariant point). Another well-known one-component system is the system H_2O. Ice has f = 2, melting ice has f = 1 and ice, water and steam (f = 0) may be in equilibrium at the unique P and T values of the triple point of H_2O.

3.8.2.1 Phase Rule in Reactive Systems

Consider a system with N phase components (chemical species), some inert, some at reaction equilibrium. R is the number of independent reactions and p the number of phases.

number of variables: p(N + 1)

number of equations: (N + 2)(p − 1) + R

R = number of conditions of reaction equilibrium $\sum \nu\mu = 0$

$$\mathbf{f} = \mathbf{n_x} - \mathbf{n_e} = \mathbf{N} - \mathbf{R} + \mathbf{2} - \mathbf{p} \tag{3.38}$$

An example; the mineral assemblage Grt + Crd + Sil + Qtz consists of four phases and we may consider seven phase components (garnet: Grs, Prp, Alm; cordierite: Fe–Crd, Mg–Crd; sillimanite: Sil; quartz: Qtz). The seven phase components are related by two independent reactions (net transfer: 2 Alm + 5 Qtz + 4 Sil = 3 Fe–Crd; exchange: $FeMg_{-1}$ (Grt) = $FeMg_{-1}$ (Crd)). The variance of the assemblage calculated from Eq. (3.38) is 3. This means that the system of equations has a unique solution if three variables can be specified independently. If, for example, the Alm and Prp content of the garnet and the Fe–Crd content of the cordierite were measured in a rock containing the four minerals in equilibrium, then the system is uniquely defined and the equilibrium pressure and temperature can be calculated. By defining c = N–R, the two forms of the phase rule become formally identical. The number of components in the sense of the phase rule is therefore taken as the total number of phase components (chemical species) minus the number of independent reaction equations between them. In the example used above, the number of system components is five (seven phase components—two independent reactions). Simple oxide components are often selected as system components and the five components CaO–MgO–FeO–Al_2O_3–SiO_2 (CMFAS) define the composition space of the Grt + Crd + Sil + Qtz rock. For a comprehensive treatment of the composition space and reaction space see Thompson (1982a, b). The phase rule derivation has been adapted from Denbigh (1971).

3.8.3 Construction of Phase Diagrams for Multicomponent Systems After the Method of Schreinemakers

A binary system of four phases is, according to the phase rule, invariant. The four minerals may occur at a unique pair of T and P (or any other two intensive variables). Graphically the four-phase assemblage occurs at a point (invariant point) for example on a P–T diagram. From this point four univariant assemblages represented by univariant lines (curves) radiate into the P–T plane (surface). The univariant lines are characterized by the absence of one of the phases occurring at the invariant point and divide the P–T plane in four divariant sectors. Each of these sectors is characterized by one unique two-phase assemblage that occurs in only one sector. The geometric distribution of univariant and divariant assemblages follows strict rules that can be derived from chemical thermodynamics. These rules

were formulated by F.A.H. Schreinemakers, in a series of articles between 1915 and 1925 and are known today as **Schreinemakers rules**. Figure 3.25a shows the geometry of the general binary four-phase system and Fig. 3.25b represents a specific geologic example. For three-component five-phase systems and complications arising from compositional degeneracies, the reader is referred to Zen (1966).

The general geometry of the binary system (Fig. 3.25a) shows an invariant assemblage of four phases with the compositions 1, 2, 3 and 4 in the two-component system a–b. The space around the invariant point is divided into four sectors by four univariant curves. Each of these curves is characterized by the absence of one phase of the invariant four-phase assemblage. The name of the absent phase is enclosed by brackets. The sectors contain either two, one or no metastable extension of the four univariant curves. The sector between the curves (2) and (3) contains two metastable extensions and is characterized by the presence of the divariant assemblage 1 + 4 which occurs only in this sector. The assemblage contains the most a-rich and the most b-rich phase, respectively. If the sector boundary (3) is crossed, 1 + 4 form phase 2, which is a new phase of intermediate composition (3 does not participate in the reaction, (3) is absent). If the sector boundary (1) is crossed, 3 forms from 2 + 4 (1 is absent). In the sector between (1) and (4), three two-phase assemblages may be present depending on the relative proportions of the components *a* and *b* in the rock. However, only one of the three assemblages is unique for the sector, namely 2 + 3. Crossing the sector boundary (4), phase 2 decomposes to 1 + 3 (4 does not participate in the reaction). Finally, crossing univariant curve (2) removes 3 by the reaction 3 = 1 + 4.

Figure 3.25b shows a specific geologic example (see also Figs. 3.1, 2.14). In rocks containing excess quartz and K-feldspar and for H_2O-saturated conditions, the four minerals garnet, cordierite, biotite and sillimanite can be represented in a binary chemographic diagram. The diagram is a projection through quartz, K-feldspar and H_2O (and parallel to the $MgFe_{-1}$ exchange vector). The geometry shown for the general binary case in Fig. 3.25a may be readily translated into Fig. 3.25b. The unique divariant assemblage for each sector is shaded in Fig. 3.25b. Note, however, that some assemblages. e.g. garnet + biotite, occur in more than one sector. Any assemblage occurring in two sectors (in the binary case) contains the phase which is absent at the sector boundary (biotite in our case). This is because biotite + garnet is not affected by the biotite-absent reaction Crd = Sil + Grt. Also note for instance, that in the cordierite-absent reaction Bt + Sil = Grt, the assemblage containing biotite must be in the sector that is not bounded by the biotite-absent reaction, and garnet must be in the sector that is not bounded by the garnet-absent reaction. This is a general rule and must be obeyed by all univariant assemblages along any of the curves.

Once the correct sequence and geometry of univariant assemblages is established around an invariant point the sequence may be translated into pressure–temperature space (Fig. 3.25c).

Three of the four reactions in our example are dehydration reactions. It is fairly safe to assume that H_2O is released from biotite as temperature increases. The

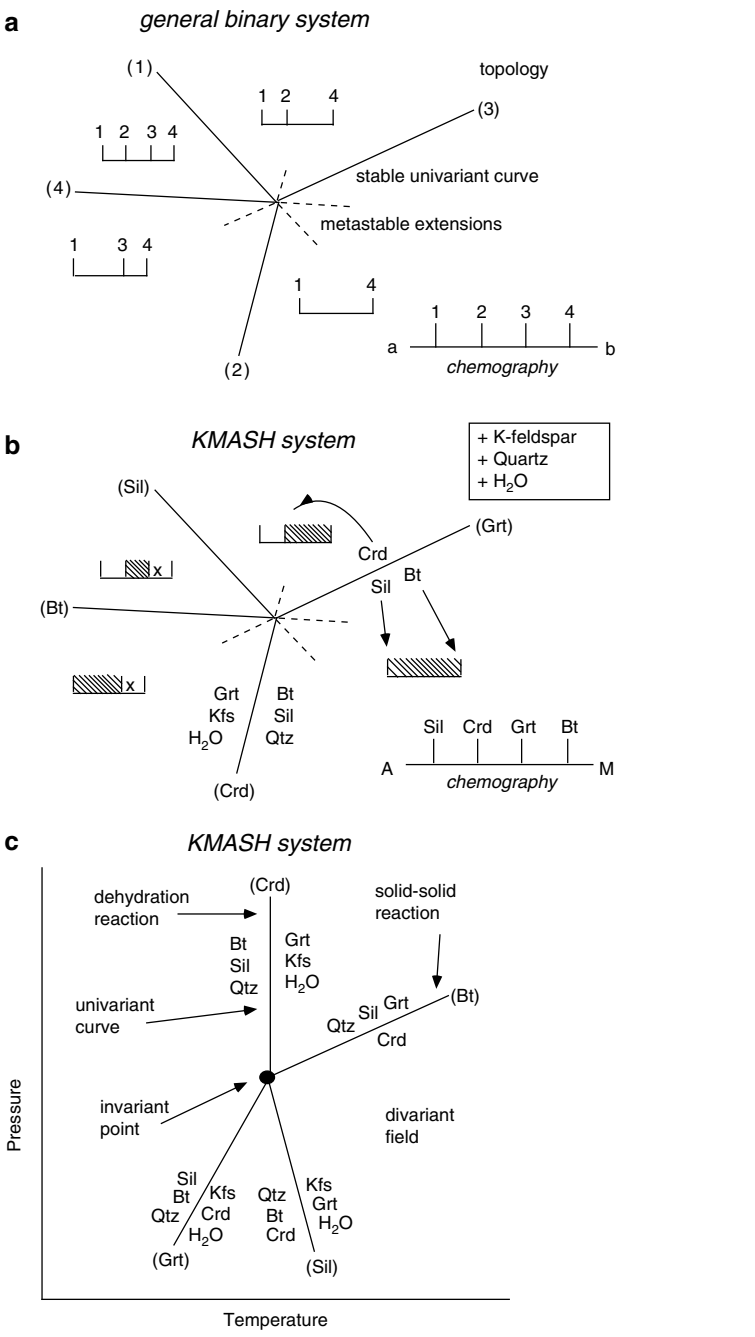

Fig. 3.25 **a** Schreinemakers diagram for general binary four phase assemblages, **b** example assemblage, Sil, Fe-Crd, Fe-Grt, and Fe-Bt projected from K-feldspar, quartz and H_2O (see also Figs. 2.14), 3.1), **c** conversion of the relationships shown in **b** to the *P*–*T* space

reactions (Crd), (Grt) and (Sil) should therefore be arranged in such a way that H_2O appears on the high-temperature side of the univariant curve. In addition, dehydration reactions commonly have steep slopes on *P–T* diagrams. Two solutions are possible; (1) the (Crd) reaction extends to high pressures from the invariant point (the reactions (Grt) and (Sil) extend to the low-pressure side), or (2) (Crd) extends to low pressures. Both solutions are geometrically correct. Solution (1) is shown in Fig. 3.25c because cordierite is a mineral that typically occurs in low- to medium-pressure metapelites. In solution (2), cordierite is restricted to high pressures, which is not consistent with geological observations. The slope of the solid–solid reaction (Bt) cannot be constrained in a way similar to that for the dehydration reactions. However, it must extend from the invariant point into the sector between (Sil) and the metastable extension of (Grt). This follows from Fig. 3.25b. Therefore, it may have a positive or a negative slope. The equilibrium of the reaction is in reality rather independent of temperature and it represents an example of a geologic barometer.

The geometric arrangement of univariant curves around invariant points on any kind of phase diagram must be strictly consistent with Schreinemakers rules. Part II, on progressive metamorphism of various rock types, provides many examples of Schreinemakers bundles in two- and three-component systems on various types of phase diagrams.

Once the correct arrangement of univariant curves around an invariant point is known the connection of this invariant point to other (if any) invariant points in the system can be examined. If, for example, spinel needs to be considered in the example used, five invariant assemblages exist in the system. The one already considered was Grt + Crd + Bt + Sil that is characterized by the absence of spinel and the invariant point of Fig. 3.25 is consequently the [Spl] absent invariant point. According to the phase rule, the system has a variance of −1. Systems with negative f-values are called **multisystems** where more than one invariant assemblage exists. Some of the invariant assemblages may be stable, others are metastable. In general, the minerals of a multisystem cannot all simultaneously coexist at equilibrium. On phase diagrams multisystems are characterized by the presence of more than one, and usually several invariant points.

A simple example can be made by reconsidering the phase relationships shown in Fig. 3.22 where the minerals pyrite, pyrrhotite, hematite, magnetite and an H_2O-fluid in the four component system Fe–O–H–S are depicted. It follows from the phase rule that f = 1. Under isobaric isothermal conditions (*P* and *T* fixed), f = −1 and five invariant assemblages exist. In the presence of an H_2O-fluid, there are four invariant assemblages involving three minerals each and lacking one mineral. Consequently, the invariant assemblages are [Po], [Py], [He] and [Mag]. As shown in Fig. 3.26, the pair [Po][He] is stable and [Mag][Py] is metastable at the selected *P–T* conditions. Note that the univariant curves change their stability level at invariant points as indicated by different dashes of the metastable extensions of the stable curves. The Schreinemakers rules are also observed by the metastable invariant points, e.g. [Py]. Also note that the metastable invariant point [Mag] is inside the field of stable magnetite and that the metastable invariant point [Py] is

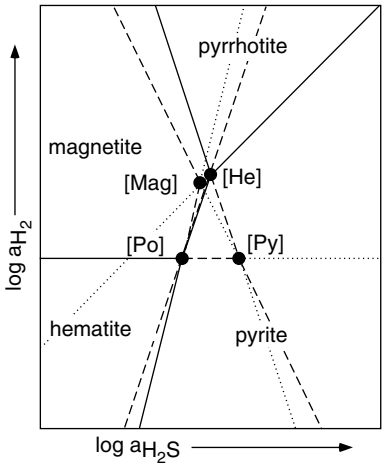

Fig. 3.26 Qualitative phase relationships among hematite, magnetite, pyrrhotite and pyrite in a log a_{H2} versus log a_{H2S} activity-activity diagram (see also Fig. 3.22). Stable equilibria = full lines; metastable level 1 equilibria = dashed lines; metastable level 2 equilibria = dotted lines. Invariant points [Po][He] are stable; [Mag][Py] are metastable

inside the field of stable pyrite. Furthermore, there is one forbidden assemblage, namely pyrrhotite + hematite. The Po + He equilibrium has no stable sector in Fig. 3.26, because it connects as a metastable line the two metastable invariant points [Mag] and [Py].

The diagram shown (Fig. 3.26) is a schematic isobaric isothermal diagram. The positions of the invariant points depend on *P*–*T*. Also the stability level of the invariant points may change with *P*–*T*. At some conditions [Mag] and [Py] could be stable, whilst [Po] and [He] being metastable. This change is known as topology inversion. The inversion of Schreinemakers topologies can be illustrated using phase relationships in metamarlstone (Fig. 3.27). The reaction equilibria among the minerals Mrg, Ky, Clz, An in rocks containing excess Qtz + Cal meet at two stable invariant points on an isobaric *T*-a_{CO2} diagram (see also Fig. 8.2 in Chap. 8). The invariant points [Ky] and [Clz] are stable at low pressure, [An] and [Mrg] stable at high *P*. The position of the invariant points changes as a function of pressure on the diagram (Fig. 3.27). The stable low-P invariant points [Ky] and [Clz] approach each other and at 946 MPa they coincide. At this P_{inv} the topology inversion occurs and all four invariant points are simultaneously stable. At $P > P_{inv}$ the invariant points [Mrg] and [An] are stable. At $P < P_{inv}$ the mineral pair An + Mrg is stable the pair Ky + Clz is metastable. At $P > P_{inv}$ Mrg + An is metastable and Ky + Clz forms a stable assemblage (Bucher-Nurminen et al. 1983).

Metastable phase relations are not normally shown on geologic phase diagrams. However, these are sometimes useful to consider and most phase diagram software permit the construction of diagrams showing the metastable phase patterns.

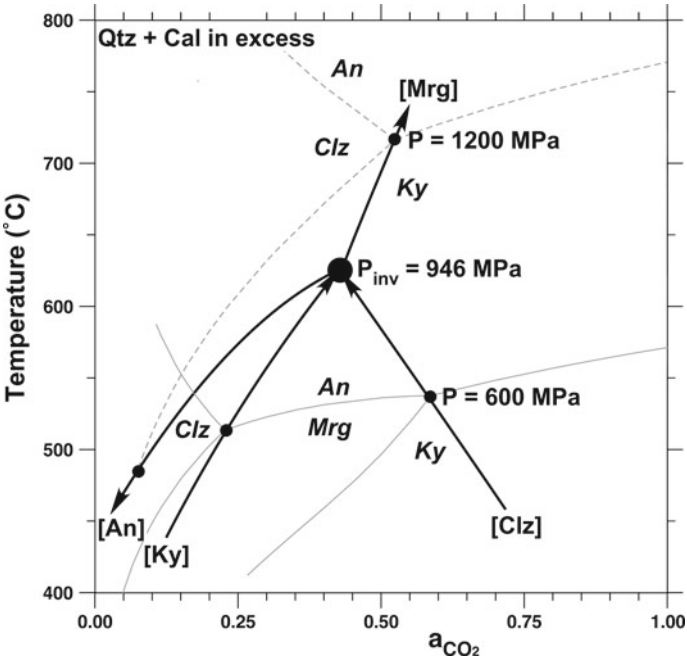

Fig. 3.27 T–a_{CO_2} model of metamorphism of metamarlstone in the system CASHC for illustration of the topology inversion (Qtz + Cal in excess). Thin gray curves = reaction equilibria among Clz, Mrg, An and Ky at the stable invariant points [Ky] and [Clz] at 600 MPa. Dashed gray curves = reaction equilibria among Clz, Mrg, An and Ky at the stable invariant points [Mrg] and [An] at 1200 MPa. Heavy black curves = positions of stable invariant points with increasing pressure. Black dots = stable invariant points. Heavy black dot = at P_{inv} = 946 MPa all invariant points are simultaneously stable = P of topology inversion P_{inv}

3.8.4 Use of Phase Diagrams, an Example

A phase diagram relevant for discussing metamorphism of carbonate rocks is used as an example to explain general properties and the use of phase diagrams. Metamorphism of marbles and carbonate-rich rocks will be presented in more detail in Chap. 6.

An isobaric T–X_{CO_2} diagram (Fig. 3.28a) shows stable mineral assemblages in siliceous dolomites. Calcite and dolomite are present in excess (however, dolomite is replaced by brucite or periclase in the upper left area of the diagram) and each field on the diagram is characterized by one diagnostic mineral. The diagram can be understood as a map showing at each point the mineral with the lowest Gibbs free energy that coexists with calcite and dolomite and a fluid of the composition given along the x-axis at the temperature given along the y-axis and at a pressure of 200 MPa. The field boundaries shown in Fig. 3.28 represent reaction equilibria of mixed volatile reactions (see Sect. 3.6.2.3). The shapes of the curves correspond to those shown in Fig. 3.19 and they are given by the stoichiometry of the reactions.

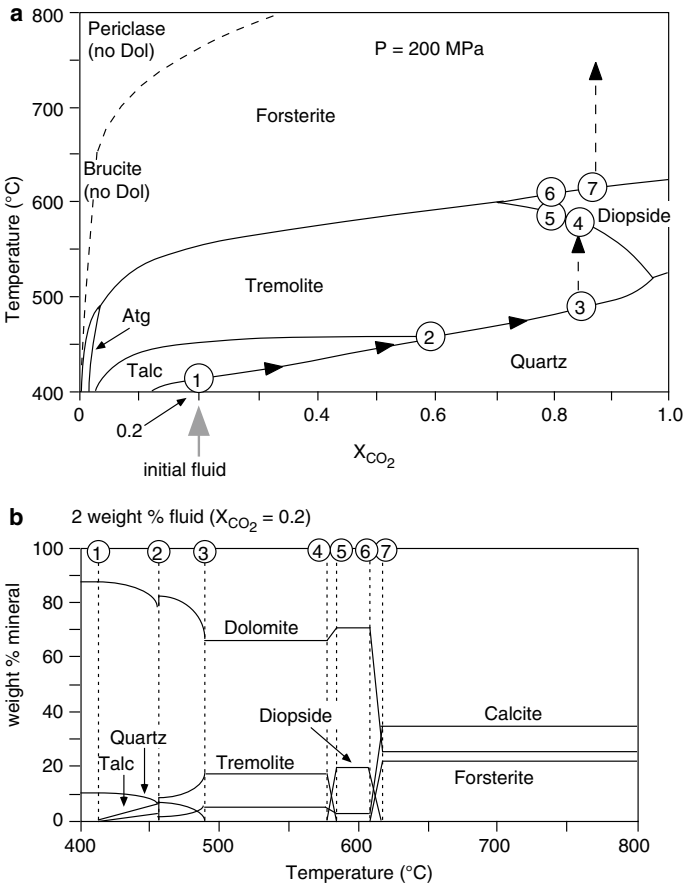

Fig. 3.28 **a** quantitative model for isobaric metamorphism of siliceous dolomites in terms of a quantitative isobaric *T-X* diagram, **b** modal composition versus *T* diagram. The diagram has originally been calculated using the computer code EQUILAS written by Brown and Skinner (1974)

The equilibrium curves terminate at intersections with other equilibria (invariant points, see also Sect. 3.8.2) or they end at the boundaries of the selected parameter window. Only stable sections of reaction equilibria are shown; metastable equilibria have been omitted.

How can this figure be used for practical purposes? Before using this figure one must be convinced that the pressure of 200 MPa is significant to the actual geological situation of interest and that a binary CO_2–H_2O fluid was present during petrogenesis. If this is accepted, then two types of simple applications are obvious:

(1) Given a marble with calcite + dolomite + diopside, at what possible *T-X* pairs was this rock stable? The answer would be: temperature was above 520 °C and below 630 °C and X_{CO_2} was greater than 0.7. An independent estimate of the

temperature at which the marble equilibrated can be made from Cal-Dol thermometry (see Chap. 4). If the temperature estimate for the rock is 550 °C, then it follows that the diopside marble indicates the presence of an extremely CO_2-rich fluid (>93 mol% CO_2). If the diopside marble is the product of prograde metamorphism, what were the possible precursor assemblages? The answer: either Tr + Cal + Dol or Qtz + Cal + Dol.

(2) Given that a temperature of about 500 °C has been reached during contact metamorphism at a certain distance from the contact of a granite pluton. The temperature may be determined, for example, from theoretical thermal modeling, from assemblages in other associated rocks of different composition, from fluid inclusion data, from Cal–Dol thermometry or from stable isotope data. What kind of marbles can be expected? The answer: tremolite marble is the obvious candidate. Quartz may still be present in rocks with an unusually CO_2-rich fluid. Forsterite marble is possible but it would require an extremely H_2O-rich fluid to form. If forsterite marble is present at this locality, one would suspect that it formed as a result of infiltration of an external fluid (see Fig. 3.24). This is even more likely for the assemblage Fo + Brc + Cal close to the $X_{CO_2} = 0$ axis.

The phase diagram (Fig. 3.28a) can also be used to deduce complete paths of prograde metamorphism taken by a particular marble sample, e.g. a marble containing initially 88 wt.% dolomite, 10 wt.% quartz and 2 wt.% fluid (with the composition 20 mol% CO_2 and 80 mol% H_2O). The question is, what will happen to this rock if it is progressively heated to 800 °C? The following discussion assumes that the volatile components released by the reactions are taken up by the fluid and remain in the rock. When heated, the model marble starts its reaction history at point (1) where talc becomes stable. The rock will be buffered along the talc field boundary by the talc-producing reaction exactly analogous to that explained in Sects. 3.6.2.3 and 3.7. How far the metamorphic path follows the talc field boundary can be calculated from the initial composition of the marble and the reaction stoichiometry (see Sect. 3.7). In the present example, the path reaches the invariant point Tlc + Tr + Qtz (point (2) in Fig. 3.28a). At this point, all previously formed talc is converted to tremolite. The path then continues along the tremolite field boundary until all quartz is used up by the tremolite-producing reaction at point (3). With continued heating, the Tr + Dol + Cal marble crosses the divariant field until diopside production sets in at point (4). All tremolite is then converted to diopside along the diopside field boundary. At point (5), the marble runs out of tremolite and at point (6), it reaches equilibrium conditions with forsterite. Forsterite replaces diopside between points (6) and (7) and at point (7) diopside has disappeared from the marble. With further heating, the Fo–Dol–Cal marble is simply heated through the divariant forsterite field to its final temperature of 800 °C.

The modal composition of the marble at any point along the reaction path in Fig. 3.28a can be calculated in the same way as in Sect. 3.7 for the wollastonite reaction. Figure 3.28b shows changes in the modal composition of the marble with increasing temperature. The specific metamorphic mileposts along the path are labeled from (1) through (7). The markers correspond to those in Fig. 3.28a:

(1) onset of continuous talc production; (2) talc disappears and significant modal amounts of tremolite are produced by the reaction at the invariant point; (3) last quartz disappears; (4) onset of continuous diopside production; (5) the rock runs out of tremolite; (6) onset of continuous forsterite production; (7) rock runs out of diopside. The end product of metamorphism is a high-grade forsterite marble with 25% Fo, 38% Cal, 32% Dol and fluid.

The two types of diagrams are helpful tools for the study of metamorphic rocks. The equilibrium phase diagram (Fig. 3.28a) relates the assemblages to the conditions under which they have formed, the composition phase diagram illustrates modal changes resulting from reactions in a rock of specific composition (Fig. 3.28b). Note however, that Fig. 3.28b is a special variant of a composition phase diagram because it combines composition with the intensive variable temperature, and is in fact a mixed variable diagram. On the other hand, a T– X_{CO_2} diagram is not a mixed variable diagram because the CO_2 and H_2O represented along the x-axis are actually related to the chemical potential of the two volatile species. Chemical potentials are intensive variables like temperature and pressure.

The model metamorphism outlined above is truly prograde. This means that with progressive metamorphism the rock (in this case, marble) advances from low to high temperature (= prograde), in which case, the rock increases in metamorphic grade and metamorphism becomes more intense (see Chap. 4). Along the reaction path, the rock maintains equilibrium at all times and one stage follows the next in a continuous series. The highest grade end-product of metamorphism is a forsterite marble that went through all lower grades in a succession of continuous prograde transformations. An inverse equilibrium path from high to low temperature would be progressively retrograde. However, retrograde metamorphism very rarely follows an equilibrium path in contrast to prograde metamorphism which produces its own fluid phase.

As a final remark, the metamorphism of a model marble illustrated in Fig. 3.28 can be understood in both a temporal or spatial sense. The former describes the metamorphic reactions experienced over time by a volume of rock at a given position in space. In the latter case the metamorphic reactions explain the mineral distribution and content of the maximum grade reached by all marble in an area. An example of the spatial viewpoint would be: from Fig. 3.28 it follows that a contact metamorphic aureole (200 MPa) in dolomitic country rock of a granite will show a regular systematic zonation with minor talc in the outermost (coldest) parts, followed by a zone of tremolite marble, a narrow zone with diopside marble and, closest to the contact with the granite (the heat source), a zone of forsterite marble. In contrast, the time aspect is exemplified in the following: a specific small outcrop of forsterite marble formed from diopside marble, which earlier was a tremolite marble that formed initially from talc marble which originated from the sedimentary siliceous dolomitic limestone protolith.

3.9 Reaction Kinetics and Chemical Transport

3.9.1 General Comments

Metamorphism of rocks occurs because external forces remove them from the equilibrium state. Rocks respond to mechanical forces by deformation. Changing *P*–*T* and chemical forces promote chemical reactions in rocks, which attempt to restore the equilibrium state. Frequently metamorphic reactions do not run to completion and textural evidence of a progressing reaction remains.

An example of a stalled chemical reaction is shown in Fig. 1.2. The texture of the Grt-Hbl schist suggests that Grt grows primarily at the expense of Chl by a mineral reaction that involves additional minerals. The reaction occurred in response to increasing *T*. It required probably a certain amount of overstepping of the equilibrium *T* for starting the reaction (Fig. 3.10). Once in progress the reaction proceeded at certain rate. The reaction rate is generally a complex function coupled to the *T*-increase with time. The surface controlled reaction rate describes the mass change (in the example mass of Grt) per unit surface area and time. In the simplest case the rate remains constant und the reaction progresses until one of the reactants has been used up.

The components that build up the new Grt must be available at the reaction site, that is, at the surface of the growing Grt. This is typically the case in the early stages of the reaction. However, later the immediate surroundings of the garnet become depleted with the reactant Chl. Therefore Chl must be dissolved in the fluid making the reaction possible at some distance from the growing Grt. The required components for Grt growth must then be transported to the Grt surface over a certain distance (Fig. 1.2). The distance for diffusional transport increases with time. The driving force for the diffusion of a component is a gradient in its chemical potential between the site of dissolving Chl and the site of the growing Grt. From the texture of the Grt-Hbl schist it can be concluded that Grt growth rate, once the reaction started running, is controlled at the early stages by the reaction kinetics and later by diffusion.

Most chemical processes in metamorphic rocks particularly the local development of metamorphic textures include a diffusional transport component (e.g. Figs. 1.1, 1.7, 8.17). Examples of diffusional processes include formation of symplectite textures e.g. Crd + Opx symplectite replacing Grt (Fig. 7.16) and formation of corona textures (Fig. 9.1b) and many other small scale redistribution of components in rocks or minerals. Modeling diffusional processes in metamorphic rocks helps to understand the development of local transport controlled textures in rocks such as corona textures (e.g. Markl et al. 1998) or the formation of blackwall rocks between rocks of incompatible compositions (Figs. 1.7, 3.4) (e.g. Bucher et al. 2005).

3.9.2 Propagation of Reaction Fronts

Metamorphic rocks often develop by reaction of components dissolved in an invading aqueous fluid with a preexisting rock not containing this component (or small amounts only). The process is termed metasomatism indicating that the original rock and the rock resulting from the process have a different composition.

Particularly impressive and clear examples of metasomatism are reaction veins in dolomite marbles at the E-rim of the Bergell granitoid intrusion (Fig. 3.29). The original rock is a coarse-grained dolomite marble that has been recrystallized during contact metamorphism by the granite (Bucher 1998). The rock contains small amounts of calcite, phlogopite, clinohumite, and spinel in imperceptible or indistinct layers perpendicular to the two reaction veins. During cooling the rocks have been repeatedly fractured and infiltrated by a hot aqueous fluid from the granite. The dissolved silica reacted along the fractures with Dol forming Ol (Fo) + Cal veins at about 550 °C and later Tr + Cal veins at 450 °C. The vein rocks contain 38 vol.% Fo + 62% Cal and 71% Tr + 29% Cal respectively showing that they formed by simple stoichiometric reactions of SiO_{2aq} with Dol. The modal composition of the produced vein rocks shows that dissolved silica is the only imported solute in the process (disregarding a small amount of Fe).

The reaction probably started rapidly at the fluid-rock interface because of the large disequilibrium between infiltrating fluid and rock. Vein growth can then be modeled using a set of equations describing reaction kinetics and diffusion (Fig. 3.30). For details see (Bucher 1998). At the early stages of vein formation the growth was controlled by the kinetics of the surface reaction. With the advancement of the reaction front from the central fracture into the pure dolomite marble

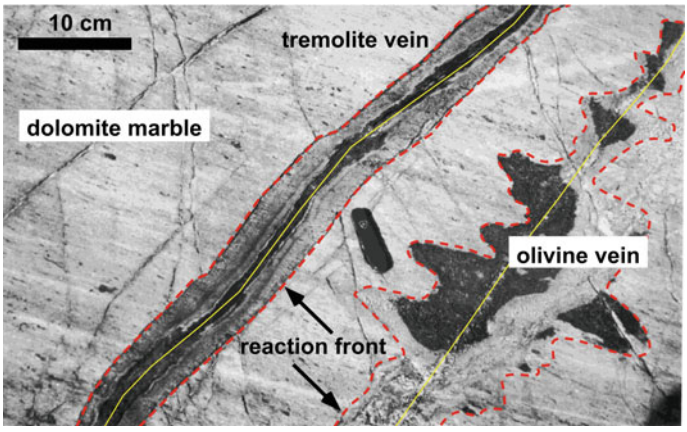

Fig. 3.29 Reaction veins in dolomite marble. Pure dolomite marble has been replaced by a tremolite + calcite vein with straight reaction fronts and a forsterite + calcite vein with strongly undulating reaction fronts (note: the vein is wet in patches and thus dark in color). Reaction fronts highlighted as dashed red boundaries between dolomite and silicate + calcite rocks. Central water-conducting fracture marked in yellow (Bucher 1998)

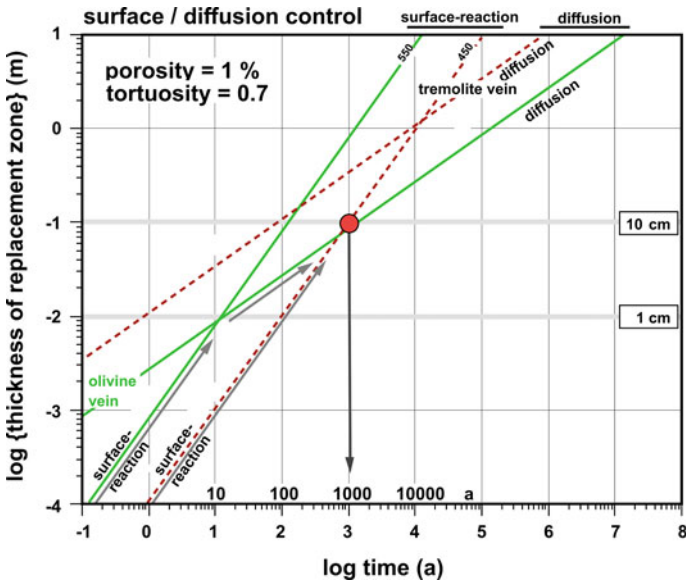

Fig. 3.30 Growth model of reaction veins in dolomite marble (Bucher 1998). Produced amount of metasomatic rock (expressed as log vein thickness) vs. log time for the two veins shown in Fig. 3.29 (tremolite vein in red, olivine vein in green). The two veins are of similar thickness (~10 cm). The green and red evolution paths meet at the red dot. Thus the growth of the Tr + Cal vein was controlled by the kinetics of the surface reaction, whilst the Ol + Cal vein was diffusion controlled after the vein has been 1 cm thick. The red dot marks the final position of the reaction front after about 1000 years of reaction. The Tr vein formed at 450 °C, the Ol vein at 550 °C

transport of dissolved silica from the fracture to the reaction front increased. After a certain time lapse the long transport distance slowed the vein forming process. Vein growth changed from being surface reaction control to diffusion control (Fig. 3.30). The reaction–diffusion crossover point is reached after 10 years in the Ol vein and after 10,000 years in the Tr vein. Thus typical veins of ~20 cm thickness (10 cm each half size) grow for about 1000 years. Ol veins are diffusion controlled most of the time, whilst Tr veins grow reaction controlled. Tr veins reach the crossover point not before they arrive at about one m thickness from center to reaction front. The wavy front surface of the Ol-vein indicates that the transport properties of the weakly layered Dol marble vary along the vein. The straight reaction front of the Tr-vein relates to the independence of the reaction kinetics from the weak sedimentary layering of the marble with Dol present in excess.

3.9.3 Diffusion in Garnet

Diffusion of chemical components is important in intercrystalline processes as in the example of the Chl–Grt reaction (Fig. 1.2). It is also important for the modification of intracrystalline chemical composition and structure of metamorphic

minerals. The classic example is the internal composition patterns in garnet porphyroblasts. Typically, garnet develops prominent and significant chemical zoning during growth. Particularly garnet porphyroblasts in metapelitic rocks often show characteristic chemical growth zoning during prograde metamorphism. In high-grade garnets the original growth zoning may be erased by intracrystalline diffusion. Continued garnet growth during retrograde metamorphism may add additional complexity to the internal chemical structure of garnets. These compositional features have attracted a cornucopia of petrologic research (a few examples: Harte and Henley 1966; Yardley 1977; Carlson 2006; Ganguly 2010; Gaidis et al. 2020; Dempster et al. 2020).

An example of compositional patterns in garnet that formed by both inter- and intracrystalline diffusion is shown on Fig. 3.31. The figure displays a fractured granulite facies Fe–Mg garnet (G-garnet) with fractures healed by new eclogite facies Ca-rich garnet (E-garnet). Thus intercrystalline diffusion occurred between the two different garnets and intracrystalline diffusion is responsible for the composition pattern from the grain contact towards the interior of the two different garnets. A section across fragments of G-Grt and E-garnet veins for the main Grt components is shown on Fig. 3.32. It is evident that the Ca concentration changes abruptly across the garnet grain boundary suggesting that Ca diffusion is very slow and the discontinuity is preserved. This is in sharp contrast to the Mg concentration, which shows a distinct diffusion pattern consistent with diffusion of Mg from G-garnet to E-garnet across the garnet boundary and within the two different garnets. The Mg-concentration versus distance data can be modeled for derived *P–T* conditions during E-garnet formation (Bucher et al. 2019); using diffusion coefficients by Carlson (2006). The observed Mg-profile required ~10 Ma to develop along the cooling path of the rock from ~580 to 530 °C. The diffusing Mg vacates its site in the G-garnet, which is in turn refilled by Fe from E-Grt in order to maintain charge balance in the garnet. This leads to very sharp Fe-discontinuities at the contact of the two garnets and increasing Fe concentrations in G-garnet towards the contact (this can also be clearly seen as bright rims around G-garnet fragments in Fig. 3.31a). Thus Fe diffuses against its own concentration gradient from low to high concentration. The process is known as uphill diffusion. The fast-diffusing Mg forces Fe to this pattern. The diffusivities are related to the ionic radii (Mg 57; Fe 63: Mn 66: Ca 100 pm = picometer = 10^{-12} m).

An unusual concentration pattern in garnet is oscillatory zoning occurring typically in Ca-rich garnets in skarn rocks. The garnets show regular recurrences of grossular and andradite rich zones (Jamtveit 1991; Holten et al. 2000). The pattern forms during garnet growth and is only moderately modified by latter diffusional processes.

Inhomogeneous composition of minerals grains subject to diffusional processes is not an exclusive feature of garnets but occurs in many other minerals as well. Alkali-feldspars for example may undergo spontaneous spinodal decomposition if cooled below the miscibility gap. K–Na feldspar unmixes into two feldspars one

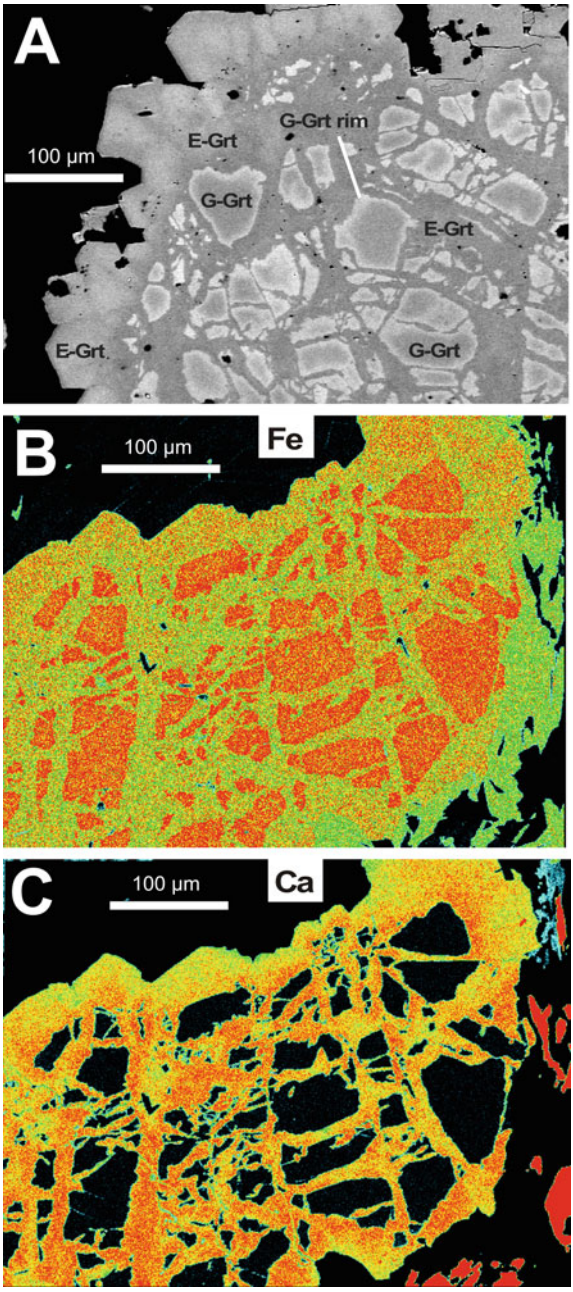

Fig. 3.31 Garnet porphyroblasts in Variscan granulite with Alpine eclogite facies garnet formed in fractures and overgrowing old Grt in rocks of the Zermatt-Saas unit of the Western Alps (Bucher et al. 2019): **a** BSE image of porphyroblast rim showing fragmented granulite facies garnet (G-Grt) and eclogite facies garnet (E-Grt) overgrowing G-Grt. Note: Bright rim around G-Grt fragments. **b** Element map for Fe showing Fe-rich G-Grt fragments and Fe-poor E-Grt. **c** Element map for Ca showing very Ca-poor G-Grt fragments (black) and Ca-bearing E-Grt rich in grossular component

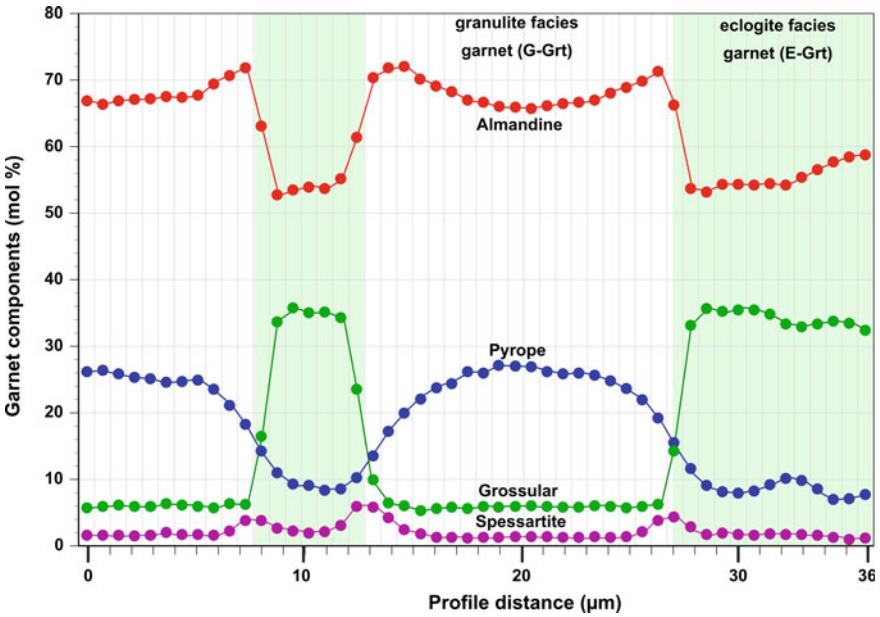

Fig. 3.32 Garnet composition along a section across a Grt porphyroblast with G-Grt fragments and E-Grt overgrowth (Fig. 3.31). E-Grt highlighted in light green. The Grt grain boundaries are marked by the three Mn maxima. Sharp discontinuities for slow diffusing Ca in distinct contrast to the typical diffusion profile of fast diffusing Mg. Note Fe-increase in G-Grt towards the contact with low Fe in E-Grt typical of uphill diffusion caused by charge balance requirements (see bright rims of G-Grt in Fig. 3.31a)

K-rich and the other Na-rich. In perthitic feldspar albite-rich of lamellae or droplets unmix and grow from homogeneous alkali feldspar. In this process Na diffuses from low concentration to high concentration and is thus another example of uphill diffusion.

References and Further Reading

Cited References

Anderson GM, Crerar DA (1993) Thermodynamics in geochemistry: the equilibrium model. Oxford University Press, New York, p 1993

Balling NP (1985) Thermal structure of the lithosphere beneath the Norwegian-Danish basin and the southern baltic shield: a major transition zone. Terra Cognita 5:377–378

Berman RG (1988) Internally-consistent thermodynamic data for minerals in the system: Na_2O-K_2O-CaO-MgO-FeO-Fe_2O_3-Al_2O_3-SiO_2-TiO_2-H_2O-CO_2. J Petrol 29:445–522

Berman RG (1991) Thermobarometry using multi-equilibribrium calculations: a new technique, with petrological applications. Can Mineral 29:833–856
Berman RG, Brown TH, Perkins EH (1987) GEØ-CALC: Software for calculation and display of pressure—temperature—composition phase diagrams. Am Mineral 72:861
Brown GC, Mussett AE (1981) The Inaccessible Earth. Allen & Unwin, London, 235 pp (p 152, Fig.8.15)
Brown TH, Skinner BJ (1974) Theoretical prediction of equilibrium phase assemblages in multicomponent systems. Am J Sci 274:961–986
Bucher-Nurminen K, Frank E, Frey M (1983) A model for the progressive regional metamorphism of margarite-bearing rocks in the Central Alps. Am J Sci 283A:370–395
Bucher-Nurminen K, Ohta Y (1993) Granulites and garnet-cordierite gneisses from Dronning Maud Land, Antarctica. J Metamorphic Geol 11: 691–703
Bucher K (1998) Growth mechanisms of metasomatic reaction veins in dolomite marbles from the Bergell Alps. Mineral Petrol 63:151–171
Bucher K, de Capitani Ch, Grapes R (2005) The development of a margarite-corundum blackwall by metasomatic alteration of a slice of mica schist in ultramafic rock, Lake Kvesjöen, Norwegian Caledonides. Can Mineralogist 43:129–156
Bucher K, Weisenberger T, Weber S, Klemm O (2019) Decoding the complex internal chemical structure of garnet porphyroblasts from the Zermatt area, Western Alps. J Metamorph Geol 37:1151–1169
Burnham CW, Holloway JR, Davis NF (1969) Thermodynamic properties of water to 1000 °C and 10'000 bars. Geol Soc Am Spec Pap 132:96
Carlson WD (2006) Rates of Fe, Mg, Mn, and Ca diffusion in garnet. Am Miner 91:1–11
Carmichael DM (1968) On the mechanism of prograde metamorphic reactions in quartz-bearing pelitic rocks. Contrib Miner Petrol 20:244–267
Chatterjee ND (1991) Applied mineralogical thermodynamics. Springer, Berlin, Heidelberg, New York, p 321
Clark SP (1966) Handbook of physical constants. Geological Society of America Memoir, 587 pp. Washington, DC, USA
Connolly JAD (1990) Multivariable phase diagrams: an algorithm based on generalized thermodynamics. Am J Sci 290:666–718
Connolly J (2009) The geodynamic equation of state: what and how. Geochem Geophys Geosyst. https://doi.org/10.1029/2009GC002540
Connolly JAD, Kerrick DM (1987) An algorithm and computer program for calculating computer phase diagrams. Calphad 11:1–55
De Capitani C, Petrakakis K (2010) The computation of equilibrium assemblage diagrams with Theriak/Domino software. Am Miner 95:1006–1016
Dempster TJ, Coleman S, Kennedy R, Chung P, Brown RW (2020) Growth zoning of garnet porphyroblasts: grain boundary and microtopographic controls. J Metam Geol 00:1–17
Denbigh K (1971) The principles of chemical equilibrium. Cambridge University Press, London, p 494
Diener J, Powell R (2012) Revised activity–composition models for clinopyroxene and amphibole. J Metamorph Geol 30(2):131–142
Ferry JM (1982) Characterization of metamorphism through mineral equilibria. Rev Mineral vol 10. Mineralogical Society of America, Washington, DC, 397 pp
Fletcher P (1993) Chemical thermodynamics for earth scientists. Longman Scientific and Technical, Essex, 464 pp
Fraser DG (1977) Thermodynamics in geology. In: NATO advanced study institutes series 30. D. Reidel, Publ. Co., Dordrecht NL, 410 pp
Gaidies F, Morneau YE, Petts DC, Jackson SE, Zagorevski A, Ryan JJ (2020) Major and trace element mapping of garnet: Unravelling the conditions, timing and rates of metamorphism of the Snowcap assemblage, west-central Yukon. J Metam Geol 00:1–32

Ganguly J (2008) Thermodynamics in earth and planetary sciences. Springer, Heidelberg, 501 p. ISBN: 978–3–540–77305–4

Ganguly J (2010) Cation diffusion kinetics in aluminosilicate garnets and geological applications. Rev Mineral Geochem 72:559–601

Garrels RM, Christ CL (1965) Solutions, minerals and equilibria. Freeman and Cooper, San Francisco, 450 pp

Gibbs JW (1878) On the equilibrium of heterogeneous substances. Am J Sci (trans Conn Acad) 16:343–524

Gibbs JW (1906) The scientific papers of J. Willard Gibbs, Thermodynamics. Longmans and Greed, London

Green E, White R, Diener J, Powell R, Holland T, Palin R (2016) Activity–composition relations for the calculation of partial melting equilibria in metabasic rocks. J Metamorph Geol 34 (9):845–869

Greenwood HJ (ed) (1977) Short course in application of thermodynamics to petrology and ore deposits. Mineralogical Society of Canada, 230pp, ASIN: B000EGPRNU

Guggenheim EA (1986) Thermodynamics. North-Holland Physics Pub, Amsterdam, p 390

Helgeson HC, Delany JM, Nesbitt HW, Bird DK (1978) Summary and critique of the thermodynamic properties of rock-forming minerals. Am J Sci 278A:229 pp

Helgeson HC, Kirkham DH (1974) Theoretical prediction of the thermodynamic behaviour of aqueous electrolytes at high pressures and temperatures. I. Summary of the thermodynamic/electrostatic properties of the solvent. Am J Sci 274:1089–1098

Holland TJB, Powell R (1985) An internally consistent dataset with uncertainties and correlations: 2. data and results. J Metamorph Geol 3:343–370

Holland TJB, Powell R (1990) An enlarged and updated internally consistent thermodynamic dataset with uncertainties and correlations: the system K_2O–Na_2O–CaO–MgO–MnO–FeO–Fe_2O_3–Al_2O_3–TiO_2–SiO_2–C–H_2–O_2. J Metamorph Geol 8:89–124

Holland TJB, Powell R (1998) An internally-consistent thermodynamic dataset for phases of petrological interest. J Metamorph Geol 16:309–343

Holland TJB, Powell R (2011) An improved and extended internally consistent thermodynamic dataset for phases of petrological interest, involving a new equation of state for solids. J Metamorph Geol 29:333–383

Holland TJ, Green EC, Powell R (2018) Melting of peridotites through to granites: a simple thermodynamic model in the system KNCFMASHTOCr. J Petrol 59(5):881–900

Holten T, Jamtveit B, Meakin P (2000) Noise and oscillatory zoning of minerals. Geochim Cosmochim Acta 64:1893–1904

Jamtveit B (1991) Oscillatory zonation patterns in hydrothermal grossular-andradite garnet: nonlinear dynamics in regions of immiscibility. Am Mineral 76:1319–1327

Johnson JW, Oelkers EH, Helgeson HC (1992) SUPCRT92: a software package for calculating the standard molal thermodynamic properties of minerals, gases, aqueous species, and reactions from 1 to 5000 bars and 0 to 1000°C. Comput Geosc 18:899–947

Lasaga AC, Kirkpatrick RJ (eds) (1981) Kinetics of geochemical processes. Reviews in Mineralogy, Mineralogical Society of America, Washington, DC, 398 pp

Lewis GN, Randall M (1961) Thermodynamics. Revised by Pitzer KS, Brewer L, McGraw-Hill, New York, 723 pp

Markl G, Foster CT, Bucher K (1998) Diffusion-controlled olivine corona textures in granitic rocks from Lofoten, Norway: calculation of Onsager diffusion coefficients, thermodynamic modelling and petrologic implications. J Metamorph Geol 16:607–623

Merino E, Canals À (2011) Self-accelerating dolomite-for-calcite replacement: self-organized dynamics of burial dolomitization and associated mineralization. Am J Sci 311:573–607

Moore WL (1972) Physical chemistry. Longman, London, p 977

Nordstrom DK, Munoz JL (1994) Geochemical thermodynamics, 2nd edn. Blackwell Scientific Publications, Boston, p 493

Peacock SM (1990) Numerical simulation of metamorphic pressure-temperature-time paths and fluid production in subducting slabs. Tectonics 9:1197–1211
Perkins D, Essene EJ, Wall VJ (1987) THERMO: a computer program for calculation of mixed-volatile equilibria. Am Mineral 72:446–447
Powell R (1978) Equilibrium thermodynamics in petrology, an introduction. Harper and Row, New York, 284 pp
Powell R, Holland TJB (1985) An internally consistent dataset with uncertainties and correlations: 1. Methods and a worked example. J Metamorph Geol 3:327–342
Powell R, Holland TJB (1988) An internally consistent dataset with uncertainties and correlations: 3. Applications to geobarometry, worked examples and a computer program. J Metamorph Geol 6:173–204
Prigogine I (1955) Thermodynamics of irreversible processes. John Wiley, New York, p 147
Richter B, Stünitz H, Heilbronner R (2016) Stresses and pressures at the quartz-to-coesite phase transformation in shear deformation experiments. J Geophys Res Solid Earth 121:8015–8033
Robie RA, Hemingway BS, Fisher JR (1978) Thermodynamic properties of minerals and related substances at 298.15 K and 1 bar (10^5 Pascals) pressure and at higher temperatures. US Geol Surv Bull 1452: 456 pp, reprinted 1979 with corrections
Saxena S, Ganguly J (1987) Mixtures and mineral reactions. Minerals and Rocks. Springer, Berlin, Heidelberg, New York, 260 pp
Spear FS, Peacock SM, Kohn MJ, Florence FP, Menard T (1991) Computer programs for petrologic P-T-t path calculations. Am Mineral 76:2009–2012
Stull DR, Prophet H (eds)(1971) JANAF thermochemical tables. Mat. Standards Ref Data Ser National Bureau of Standards, Washington, DC, 1141 pp
Thompson JB (1982a) Composition space; an algebraic and geometric approach. In: Ferry JM (ed) Characterization of metamorphism through mineral equilibria. Reviews in mineralogy, Mineralogical Society of America, Washington DC, pp 1–31
Thompson JB (1982b) Reaction space; an algebraic and geometric approach. In: Ferry JM (ed) Characterization of metamorphism through mineral equilibria. Reviews in mineralogy Mineralogical Society of America, Washington, DC, pp 33–52
Walther JV, Orville PM (1982) Rates of metamorphism and volatile production and transport in regional metamorphism. Contrib Mineral Petrol 79:252–257
White R, Powell R, Holland T, Johnson T, Green E (2014) New mineral activity–composition relations for thermodynamic calculations in metapelitic systems. J Metamorph Geol 32(3):261–286
Wood BJ, Fraser DG (1976) Elementary thermodynamics for geologists. Oxford University Press, Oxford, p 303
Yardley BWD (1977) An empirical study of diffusion in garnet. Am Miner 62:793–800
Zen E-an (1966) Construction of pressure-temperature diagrams for multi-component systems after the method of Schreinemakers: a geometrical approach. US Geol Surv Bull 1225:56
Zimmer K, Zhang Y, Lu P, Chen Y, Zhang G, Dalkilic M, Zhu Ch (2016) SUPCRTBL: A revised and extended thermodynamic dataset and software package of SUPCRT92. Comput Geosci 90A:97–111

Further Reading and a Selection of Additional Literature

Baxter EF, DePaolo DJ (2002) Field measurement of high temperature bulk reaction rates I: theory and technique. Am J Sci 302:442–464
Bell TH, Cuff C (1989) Dissolution, solution transfer, diffusion versus fluid flow and volume loss during deformation/metamorphism. J Metamorph Geol 7:425–448
Bell TH, Hayward N (1991) Episodic metamorphic reactions during orogenesis: the control of deformation partitioning on reaction sites and reaction duration. J Metamorph Geol 9:619–640

Bell TH, Mares VM (1999) Correlating deformation and metamorphism around orogenic arcs. Am Mineral 84:1727–1740
Bickle MJ, McKenzie D (1987) The transport of heat and matter by fluids during metamorphism. ContribMineral Petrol 95:384–392
Brady JB (1988) The role of volatiles in the thermal history of metamorphic terranes. J Petrol 29:1187–1213
Brodie KH, Rutter EH (1985) On the relationship between deformation and metamorphism with special reference to the behaviour of basic rocks. In: Thompson AB, Rubie DC (eds) Advances in physical geochemistry. Springer, Berlin, Heidelberg, New York, pp 138–179
Burt DM (1991) Vectors, components, and minerals. Am Min 76:1033–1037
Cermak V, Rybach L (1987) Terrestrial heat flow and the lithosphere structure. Terra Cognita 7:685–687
Chapman DS (1986) Thermal gradients in the continental crust. The nature of the lower continental crust. In: Dawson JB, Carswell DA, Hall J, Wedepohl KH (eds) The nature of the lower continental crust. Geological Society of London Special Publication, Blackwell, London, pp 63–70
Clarke GL, Fitzherbert JA, Milan LA, Daczko NR, Degeling HS (2010) Anti-clockwise P-T paths in the lower crust: an example from a kyanite-bearing regional aureole, George Sound, New Zealand. J Metamorph Geol 28:77–96
Davy P, Gillet P (1986) The stacking of thrust slices in collision zones and its thermal consequences. Tectonics 5:913–929
Eugster HP (1959) Oxidation and reduction in metamorphism. In: Abelson PH (ed) Researches in geochemistry. John Wyllie & Sons, New York, pp 397–426
Eugster HP (1977) Compositions and thermodynamics of metamorphic solutions. In: Fraser DG (ed) Thermodynamics in geology. Reidel, Dordrecht, pp 183–202
Eugster HP (1986) Minerals in hot water. Am Mineral 71:655–673
Eugster HP, Gunter WD (1981) The compositions of supercritical metamorphic solutions. Bull Mineral 104:817–826
Ferry JM (1980) A case study of the amount and distribution of heat and fluid during metamorphism. Contrib Mineral Petrol 71:373–385
Ferry JM (1983) Application of the reaction progress variable in metamorphic petrology. J Petrol 24:343–376
Foster CT (1999) Forward modeling of metamorphic textures. Can Mineral 37:415–429
Foster CT (1981) A thermodynamic model of mineral segregations in the lower sillimanite zone near Rangeley, Maine. Am Miner 66:260–277
Froese E (1977) Oxidation and sulphidation reactions. In: Greenwood HJ (ed) Application of thermodynamics to petrology and ore deposits, Short Course, 2, Mineralogical Association of Canada, Vancouver, 84–98
Frost BR (1988) A review of graphite-sulfide-oxide-silicate equilibria in metamorphic rocks. Rend Soc Ital Mineral Petrol 43:25–40
Frost BR (1991) Introduction to oxygen fugacity and its petrologic importance. In: Lindsley DH (ed) Oxide minerals: petrologic and magnetic significance. Reviews in Mineralogy vol.25, Mineralogical Society of America, 1–9
Fyfe WS, Turner FJ, Verhoogen J (1958) Metamorphic reactions and metamorphic facies. Geol Soc Am Mem. 73: 260pp
Fyfe WS, Price NJ, Thompson AB (1978) Fluids in the earth's crust. Elsevier, New York, p 383
Gerya T (2015) Tectonic overpressure and underpressure in lithospheric tectonics and metamorphism. J Metamorph Geol 33:785–800
Greenwood HJ (1975) Buffering of pore fluids by metamorphic reactions. Am J Science 275:573–594
Heinrich CA (1986) Eclogite facies regional metamorphism of hydrous mafic rocks in the central alpine adula nappe. J Petrol 27:123–154

Lasaga AC, Jianxin J (1995) Thermal history of rocks: P-T-t paths from geospeedometry, petrologic data, and inverse theory techniques. Am J Sci 295:697–741
Lasaga AC, Lüttge A, Rye DM, Bolton EW (2000) Dynamic treatment of invariant and univariant reactions in metamorphic systems. Am J Sci 300:173–221
Lasaga AC, Rye DM (1993) Fluid flow and chemical reaction kinetics in metamorphic systems. Am J Sci 293:361–404
Manning CE, Ingebritsen SE (1999) Permeability of the continental crust: implications of geothermal data and metamorphic systems. Rev Geophys 37:127–150
Miyashiro A (1961) Evolution of metamorphic belts. J Petrol 2: 277–311
Miyashiro A (1964) Oxidation and reduction in the earth's crust, with special reference to the role of graphite. Geochim Cosmochim Acta 28:717–729
Müller T, Baumgartner LP, Foster CT Jr, Vennemann TW (2004) Metastable prograde mineral reactions in contact aureoles. Geology 32:821–824
Munoz JL, Ludington SD (1974) Fluoride-hydroxyl exchange in biotite. Am J Sci 274:396–413
Nisbet EG, Fowler CMR (1988) Geotherms in the continental crust and metamorphism. In Nisbet EG, Fowler CMR (eds) Short course on heat, metamorphism, and tectonics. Mineral Assoc Canada Short Course 14, 34–50
Oxburgh ER (1974) The plain man's guide to plate tectonics. Proc Geol Assoc 85:299–358
Petrelli M, Perugini D (2016) Solving petrological problems through machine learning: the study case of tectonic discrimination using geochemical and isotopic data. Contrib Mineral Petrol 171:81
Petrini K, Podladchikov Yu (2000) Lithospheric pressure-depth relationship in compressive regions of thickened crust. J Metamorph Geol 18: 67–77
Sclater JG, Jaupart C, Galson D (1980) The heat flow through oceanic and continental crust and the heat loss of the Earth. Rev Geophys Space Phys 18:269–311
Skippen GB, Carmichael DM (1977) Mixed-volatile equilibria. In: Greenwood HJ (ed) Application of thermodynamics to petrology and ore deposits. Mineralogical Society of Canada, Vancouver, Short Course, pp 109–125
Spear FS (1993) Metamorphic phase equilibra and pressure-temperature-time paths. Monograph 824 Mineralogical Society of America, Washington, DC, 824 pp
Spear FS, Peacock SM (1989) Metamorphic pressure-temperature-time paths. Short Course in Geology, vol 7, American Geophysical Union, Washington, DC, 102 pp
Spear FS, Rumble D III, Ferry JM (1982) Linear algebraic manipulation of n-dimensional composition space. In: Ferry JM (ed) Characterization of metamorphism through mineral equilibria. Reviews in mineralogy, Mineralogical Society of America, Washington, DC, pp 53–104
Spear FS, Selverstone J, Hickmont D, Crowley P, Hodges KV (1984) P-T paths from garnet zoning: a new technique for deciphering tectonic processes in crystalline terranes. Geology 12:87–90
Spiess R, Bell TH (1996) Microstructural controls on sites of metamorphic reaction: a case study of the inter-relationship between deformation and metamorphism. Eur J Mineral 1:165–186
Spooner ETC, Fyfe WS (1973) Sub-sea-floor metamorphism, heat and mass transfer. Contrib Mineral Petrol 42:287–304
Stephenson BJ, Waters DJ, Searle MP (2000) Inverted metamorphism and the Main Central Thrust: field relations and thermobarometric constraints from the Kishtwar Window, NW Indian Himalaya. J Metamorph Geol 18:571–590
Tajčmanová L, Podladchikov Y, Powell R, Moulas E, Vrijmoed J, Connolly J (2014) Grain-scale pressure variations and chemical equilibrium in high-grade metamorphic rocks. J Metamorph Geol 32:195–207
Tajčmanová L, Vrijmoed J, Moulas E (2015) Grain-scale pressure variations in metamorphic rocks: implications for the interpretation of petrographic observations. Lithos 216:338–351
Thompson AB (1981) The pressure-temperature (P, T) plane viewed by geophysicists and petrologists. Terra Cognita 1:11–20

Thompson AB, England PC (1984) Pressure-temperature-time paths of regional metamorphism II. their inference and interpretation using mineral assemblages in metamorphic rocks. J Petrol 25:929–955

Thompson AB, Ridley JR (1987) Pressure-temperature-time (P-T-t) histories of orogenic belts. Philos Trans R Soc London A321:27–45

Touret JLR (2001) Fluids in metamorphic rocks. Lithos 55:1–25

Vigneresse JL (1988) Heat flow, heat production and crustal structure in peri-Atlantic regions. Earth PlanetSci Lett 87:303–312

Vigneresse JL, Cuney M (1991) What can we learn about crustal structure from thermal data? Terra Nova 3:28–34

Waters DJ, Lovegrove DP (2002) Assessing the extent of disequilibrium and overstepping of prograde metamorphic reactions in metapelites from the Bushveld Complex aureole, South Africa. J Metamorph Geol 20:135–149

Wood BJ, Walther JV (1984) Rates of hydrothermal reactions. Science 222:413–415

Yamato P, Brun JP (2017) Metamorphic record of catastrophic pressure drops in subduction zones. Nat Geosci 10:46–50